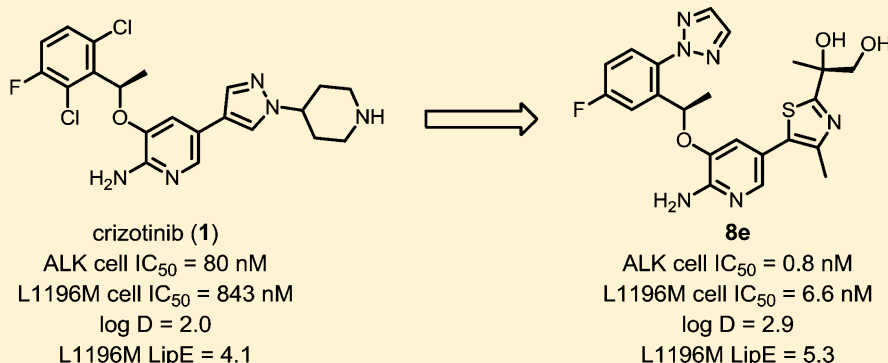


Design of Potent and Selective Inhibitors to Overcome Clinical Anaplastic Lymphoma Kinase Mutations Resistant to Crizotinib

Qinhua Huang,* Ted W. Johnson,* Simon Bailey, Alexei Brooun, Kevin D. Bunker, Benjamin J. Burke, Michael R. Collins, Andrew S. Cook, J. Jean Cui, Kevin N. Dack, Judith G. Deal, Ya-Li Deng, Dac Dinh, Lars D. Engstrom, Mingying He, Jacqui Hoffman, Robert L. Hoffman, Patrick S. Johnson, Robert S. Kania, Hieu Lam, Justine L. Lam, Phuong T. Le, Qiuhsia Li, Laura Lingardo, Wei Liu, Melissa West Lu, Michele McTigue, Cynthia L. Palmer, Paul F. Richardson, Neal W. Sach, Hong Shen, Tod Smeal, Graham L. Smith, Albert E. Stewart, Sergei Timofeevski, Konstantinos Tsaparikos, Hui Wang, Huichun Zhu, Jinjiang Zhu, Helen Y. Zou, and Martin P. Edwards

La Jolla Laboratories, Pfizer Worldwide Research and Development, 10770 Science Center Drive, San Diego, California 92121, United States

 Supporting Information



ABSTRACT: Crizotinib (**1**), an anaplastic lymphoma kinase (ALK) receptor tyrosine kinase inhibitor approved by the U.S. Food and Drug Administration in 2011, is efficacious in ALK and ROS positive patients. Under pressure of crizotinib treatment, point mutations arise in the kinase domain of ALK, resulting in resistance and progressive disease. The successful application of both structure-based and lipophilic-efficiency-focused drug design resulted in aminopyridine **8e**, which was potent across a broad panel of engineered ALK mutant cell lines and showed suitable preclinical pharmacokinetics and robust tumor growth inhibition in a crizotinib-resistant cell line (H3122-L1196M).

INTRODUCTION

Anaplastic lymphoma kinase (ALK) belongs to the insulin receptor (IR) superfamily of receptor tyrosine kinases (RTKs). Normally, ALK plays an important role in the development of the brain and exerts its effects on specific neurons in the nervous system.¹ Inhibition may be a suitable strategy, since ALK knockout mice live a normal life span without obvious abnormalities but are described as having an “anti-depressive” phenotype.²

Over the last 20 years, ALK has been associated with several cancers. The ALK gene has been shown to be oncogenic by three different mechanisms across a variety of tumors: ALK mutations, amplifications, and translocations (fusions).³ The oncogenic nucleophosmin (NPM)-ALK fusion gene was first identified in anaplastic large-cell lymphoma (ALCL) in 1994.⁴ Subsequently, multiple ALK fusions have been identified in diffuse large B-cell lymphoma (DLBCL),⁵ inflammatory myofibroblastic tumors (IMT),⁶ and non-small-cell lung carcinoma (NSCLC).⁷

Although many fusion partners exist in a variety of tumor types, echinoderm microtubule-associated protein-like 4 (EML4)-ALK represents the largest patient population, accounting for approximately 6% of NSCLC patients. Fusion of ALK with the EML4 protein was thought to constitutively activate the kinase through oligomerization of the coiled-coil domain of EML4.^{7b} In addition, amplification and oncogenic mutations of ALK in neuroblastoma,⁸ inflammatory breast cancer,⁹ and ovarian cancer¹⁰ have also been reported. Therefore, ALK has emerged as an attractive drug target for cancer therapy.

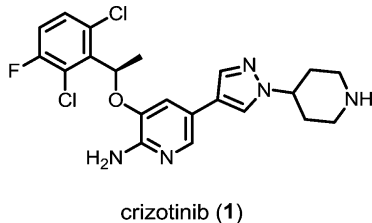
In 2011, crizotinib (**1**, brand name Xalkori) became the first ALK inhibitor approved by the U.S. Food and Drug Administration (FDA) as a first-line treatment for ALK-positive lung cancer patients.¹¹ Most ALK-fusion-positive NSCLC patients benefit significantly from crizotinib treatment, showing

Received: November 22, 2013

Published: January 16, 2014



objective response rates (complete and partial) of 60% and progression-free survival of approximately 10 months.¹² Although the initial therapeutic response is impressive, many patients eventually develop resistance to crizotinib. The tumors that progress on crizotinib have exhibited a range of resistance mechanisms, with ALK gene point mutations and insertions being well-characterized.¹³ For this reason, there is a need to develop second-generation anti-ALK therapies.



Recent encouraging phase I/II clinical results for ALK inhibitors **2** (LDK378, Novartis),¹⁴ **3** (ASP3026, Astellas),¹⁵ **4** (CH5424802, Roche/Chugai),¹⁶ and **5** (AP26113, Ariad, structure undisclosed and series exemplified as **5**)¹⁷ (Figure 1) demonstrate the promise of these classes of therapeutics to treat crizotinib-naïve and relapsed ALK-positive NSCLC patients.

Since crizotinib was originally designed as a mesenchymal–epithelial transition factor (c-MET) kinase inhibitor,^{11c} we sought to optimize its scaffold for ALK potency. Herein, we report design advances on a 3-benzylxaminopyridine scaffold toward highly potent inhibitors of ALK wild-type and resistant mutants using lipophilicity–efficiency (LipE)¹⁸ analysis and structure-based drug design (SBDD).

RESULTS AND DISCUSSION

Characterization of Crizotinib Potency against ALK Mutants. As mentioned, ALK gene point mutations and insertions were well-characterized mechanisms of resistance. The relative positions of ALK kinase domain point mutations and insertions identified from crizotinib-relapsed patient samples are illustrated in Figure 2. L1196M, G1269A, and G1202R make direct contacts with crizotinib. S1206Y is in close proximity to the crizotinib binding site, while other reported mutations, such

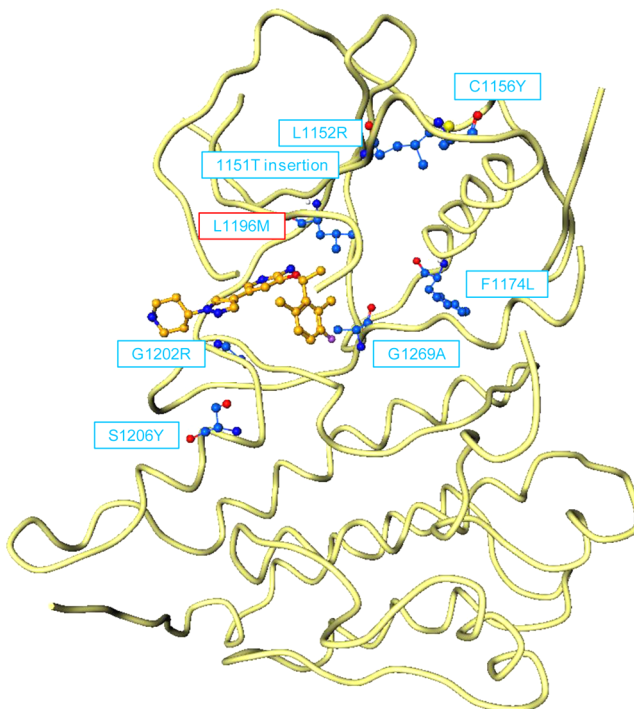


Figure 2. Crystal structure of crizotinib bound to the ALK kinase domain, showing the positions of clinically identified crizotinib-resistant mutations.

as L1152R, C1156Y, F1174L, and 1151Tins are more distal to the inhibitor.

Several engineered cell lines expressing wild-type (wt) and mutant ALK were developed to evaluate crizotinib potency. From clinical data, at the recommended 250 mg b.i.d. (twice a day) dose, the average human free plasma concentration of crizotinib is 45–70 nM, which nearly matches only the wt ALK IC₅₀ values across cell lines.¹⁹ In addition to wt ALK IC₅₀, Table 1 summarizes crizotinib inhibition activity in mechanistic and proliferation inhibition assays using engineered cell lines harboring clinically reported ALK mutations. In NIH-3T3-

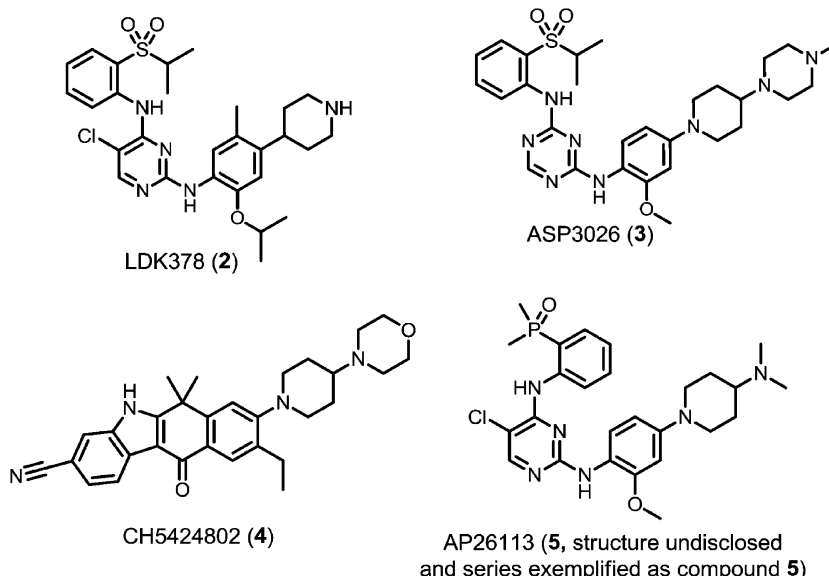


Figure 1. Structures of selected clinical ALK inhibitors.

Table 1. Cell-Based Efficacy of Crizotinib against Wild Type and Various Mutants of ALK

	ALK phospho in 3T3-EML4-ALK engineered cells (IC_{50} , nM)								ALK-fusion-driven cell proliferation (IC_{50} , nM)				
	wt	L1196M	G1269A	S1206Y	C1156Y	F1174L	L1152R	1151Tins	H3122	H2228	Karpas299	H3122-L1196M	H3122-G1269A
crizotinib	80	843	605	626	478	165	1026	3039	108	118	62	838	623

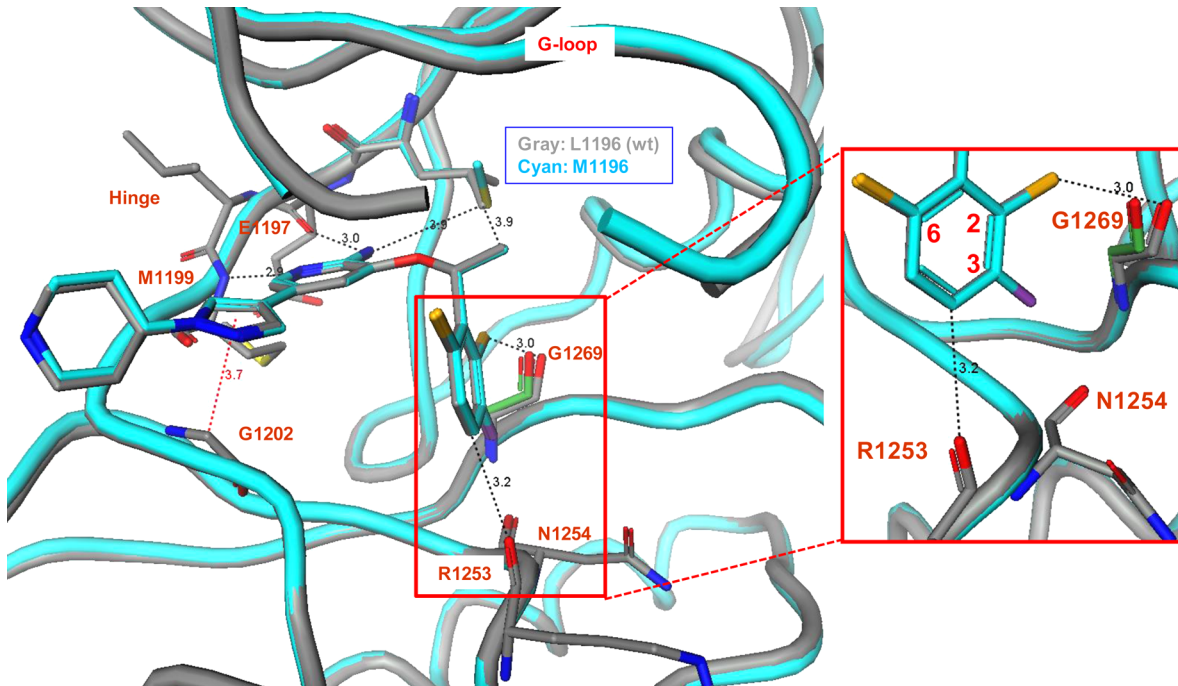


Figure 3. Co-crystal structure of crizotinib with ALK wt (gray, PDB 2xp2) overlaid with L1196M mutant (cyan, PDB 2yfx) and the G1269 residue from L1196M apo structure (green, PDB 2yhv).

ALK mutant engineered cell lines, the cell IC_{50} value for crizotinib ranges from 165 to 3039 nM, which represents a 2–38-fold shift relative to wt potency. This \times -fold shift is mirrored by antiproliferative data in wild-type lines (H3122, H2228, and Karpas299) and various mutant engineered lines (H3122-G1269A and H3122-L1196M). The concentration of crizotinib required to sufficiently inhibit these mutants substantially exceeds clinically relevant concentrations.

Because of the reported higher frequency of the methionine gatekeeper mutant from analysis of clinical samples^{13a} and significant resistance in vitro (Table 1), L1196M ALK was chosen as the sentinel mutant for both biochemical and cellular screening assays in our compound progression cascade. Once compounds of interest were identified, subsequent testing was performed on clinically reported mutants (G1269A, S1206Y, C1156Y, F1174L, L1152R, and 1151Tins) to ensure broad coverage of relevant resistant point mutants encountered in vivo.

Crizotinib–ALK Kinase Domain Co-crystal Structure Analysis. Crizotinib is a type I ATP-competitive inhibitor of c-MET and ALK. Previous publications highlight crizotinib bound to the nonphosphorylated state, autoinhibitory conformation of the c-MET kinase.^{11c} The co-crystal of the wt ALK kinase domain complexed with crizotinib (PDB 2xp2) shows a binding conformation similar to c-MET (PDB 2wgj), yet it lacks the tyrosine π – π stacking interaction observed with c-MET. This likely contributes to the modest loss in ALK potency relative to c-MET.

Co-crystal structures of wt and L1196M ALK were undertaken to identify binding interactions and protein conformations (Figure 3). The binding mode of crizotinib in both proteins is

quite similar. Crizotinib makes similar hydrogen bonds to the hinge residues M1199 and E1197 in the wt (2.9 and 3.0 Å) and L1196M (2.9 and 3.1 Å) structures. In both structures, the gatekeeper residue contacts crizotinib at the exocyclic amino group (3.9 Å in wt, 3.9 Å in L1196M) and the (R)-methyl group (3.9 Å in wt, 4.0 Å in L1196M). The pyrazole ring sits atop G1202 at similar distances (3.7 Å in wt, 3.6 Å in L1196M) and the 2,6-dichloro-3-fluorophenyl group is in a very similar position in the wt and L1196M structures. Overall protein conformations look very comparable between the two crystal structures with the exception of the L1196 to M1196 gatekeeper residue difference.

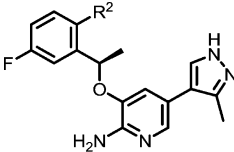
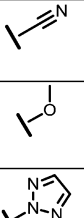
A closer look at the “head” dichlorofluorophenyl group reveals that the fluorine at C3 contributes to potency and binding efficiency by (a) filling a small hydrophobic pocket formed by the G1269 and N1254 residues and (b) polarizing the neighboring C4–H bond to productively interact with the R1253 carbonyl oxygen. A comparison of the apo structure of ALK to the crizotinib–ALK bound structure shows that the 2-chloro substituent is in close contact with the backbone carbonyl of G1269. This close contact may be unfavorable, as comparison of apo and crizotinib-bound structures shows that this carbonyl rotates (~30°) away from the inhibitor to accommodate crizotinib binding (highlighted in green, Figure 3). In contrast, the equivalent carbonyl (A1221) in the co-crystal of crizotinib (1)/c-MET (PDB 2wgj) is not in this location. There is an inversion of the amide NH and C=O orientation of the c-MET A1221 residue compared to the overlapping ALK G1269 residue, and the 2-chloro was optimized for the inverted c-MET A1221 residue.^{11c}

Table 2. Potency, ADME, and Efficiency of Crizotinib (1) and Its Des-2-chloro Analogue (1a)

	R ¹	L1196M K _i (nM)	L1196M cell IC ₅₀ (nM)	log D ^a	HLM Cl _{int,app} ^b (mL·min ⁻¹ ·kg ⁻¹)	RRCK P _{app} (A to B) ^c (10 ⁻⁶ cm/s)	LipE ^d (K _i)
crizotinib (1)	Cl	8.2	843	2.0	44	0.8	6.1
1a	H	5.0	387	1.7	27	2.3	6.6

^aLog D measured at pH 7.4.²⁰ ^bCl_{int,app} refers to the total intrinsic clearance obtained from scaling in vitro half-lives in human liver microsomes.²¹ ^cRRCK cells with low transporter activity were isolated from Madin–Darby kidney cells and were used to estimate intrinsic absorptive permeability.²² ^dLipE = −log K_i − log D.

Table 3. Potency, ADME, and Efficiency of the Substituted Fluorophenyl Head Group

Compound	R ²	L1196M Ki (nM)	L1196M Cell IC ₅₀ (nM)	log D ^a	HLM Cl _{int,app} (ml/min/kg) ^b	RRCK P _{app} (A to B) (10 ⁻⁶ cm/s) ^c	LipE ^d (K _i)
6a		16	1254	3.4 ^e	31	18	4.3
6b		11	805	2.7	37	20	5.2
6c		2.0	69	3.5	65	14	5.2
6d		2.6	60	3.3	46	21	5.3

^aLog D was measured at pH 7.4.²⁰ ^bCl_{int,app} refers to the total intrinsic clearance obtained from scaling in vitro half-lives in human liver microsomes.²¹

^cRRCK cells with low transporter activity were isolated from Madin–Darby kidney cells and were used to estimate intrinsic absorptive permeability.²² ^dLipE = −log K_i − log D. ^eclog D.

While the overall resolution of the structures is excellent, some disorder is observed. Both bound structures of crizotinib with the wt and L1196M ALK protein show disordered G-loops in the portion adjacent to the 6-Cl substituent of the headgroup. The remaining portions of the G-loop are well-defined (up to G1123 in wt ALK, up to L1122 in L1196M mutant) and are greater than 4.5 Å from the chlorine.

The pyrazolopiperidine “tail” group of crizotinib was a region of the molecule that required further optimization for ALK potency and absorption, distribution, metabolism, and excretion (ADME) properties. The pyrazole portion of the tail group filled a lipophilic pocket near the solvent-exposed region, in close proximity to G1202. The piperidinyl group pointed out toward solvent. This group added significant molecular weight and a basic amine, resulting in low in vitro permeability (RRCK = 0.8 × 10⁻⁶ cm/s) and high efflux [multidrug resistance (MDR) BA/AB = 45]. The optimization campaign focused on neutral pyrazolopiperidine tail replacements to impart improved

permeability. Strategies to optimize both the 2,6-dichloro-3-fluorophenyl head and the pyrazolopiperidine tail in crizotinib (1) will be discussed below.

Optimization of the Head Group. On the basis of the structural analyses above, we believed that a smaller substituent at C2 may complement the protein by allowing a relaxation of the G1269 carbonyl as seen in the apo structure. Furthermore, the C2 hydrogen would be polarized by the adjacent fluorine atom to complement the G1269 carbonyl oxygen. Another benefit of the des-chloro compound would be lower molecular weight and log D, providing physical properties with greater likelihood for improving pharmaceutical properties. Both crizotinib (1) and the 2-des-chloro analogue (1a) were evaluated to quantify the various effects of removing the 2-chloro group (Table 2). Indeed, the hydrogen analogue 1a exhibited improvements in potency, lipophilic efficiency, and in vitro clearance relative to the chloro analogue 1.

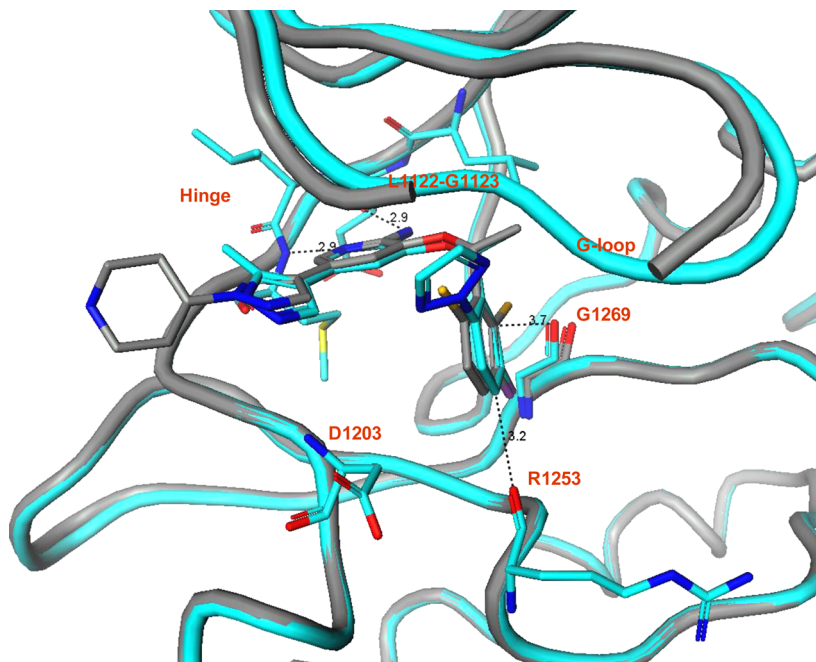


Figure 4. Co-crystal structures of crizotinib/ALK wt (gray, PDB 2xp2) and **6d**/ALK wt (cyan, PDB 4ccb).

Holding the des-chloro modification constant and utilizing a small and potent pyrazole tail moiety, a variety of fluorophenyl analogues with different R² groups (Table 3) were synthesized to identify higher LipE replacements of the 6-chloro substituent (Table 2 and Figure 3). Enzymatic LipE of the larger groups CN (**6b**), OMe (**6c**), and triazolo (**6d**) were one unit higher than the smaller fluorine analogue (**6a**). Other matched pairs containing different tail groups followed a similar trend (data not shown). In addition to lipophilic efficiency, the triazolo motif better balanced cell potency and ADME properties. For example, nitrile **6b** had similar in vitro clearance to triazole **6d** but lost more than 10-fold cell potency. On the other hand, the methoxy-substituted analogue (**6c**) had good mutant cell potency but contained a metabolically labile methoxy group displaying high in vitro clearance. Therefore, the 2-triazolo-5-fluorophenyl head group was chosen as our standard head group for tail group optimization based on balanced potency, efficiency, clearance, and permeability.

A co-crystal structure with ALK was obtained for the more potent and lipophilic efficient triazole lead (**6d**). Figure 4 shows the aligned and overlapped bound structures for triazole **6d** (cyan, 2.0 Å) and crizotinib **1** (gray, 1.9 Å) in wt ALK kinase domain. The triazole group of **6d** forms a 60° torsion angle with the phenyl ring and is positioned to make contact with the backbone of residues L1122-G1123 of the ALK G-loop. By contrast, the chloro of crizotinib does not extend far enough to make contact with the G-loop. Note that the G1269 carbonyl in the bound structure of **6d**/wt ALK (Figure 4) was relaxed, as seen in the apo structure, by removing the 2-chloro in the head group compared with the crizotinib/wt ALK bound structure.

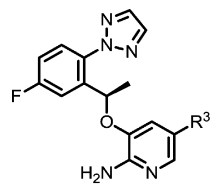
Optimization of the Tail Group. The 2-triazolo-5-fluorophenyl head group was held constant while neutral replacements for the basic pyrazolopiperidine group in crizotinib (**1**) were sought. A variety of substituted cyclic tail groups were designed, synthesized, and tested for both biological potency and ADME properties (Table 4). While **6d** exhibited good potency, it was a substrate for glucuronidation at the unsubstituted pyrazole site. Methyl-protected 4-pyrazolo analogues (**7a** and **7b**)

maintained similar enzymatic potency and LipE. Although introduction of the cyano group in **7b** did not lower lipophilicity much, it improved the in vitro clearance relative to the methyl analogue **7a**. Other molecules containing five-membered-ring R³ groups, such as **7c** and **7d**, decreased LipE approximately 0.5 units compared with the 4-pyrazolo tails (**6d**, **7a**, and **7b**). The six-membered-ring R³ group in **7f** reduced LipE by 0.4 units relative to the similar but more electron-rich group in **7e**.

In order to improve both the binding affinity and efficiency, we took a close look at protein–ligand interactions in the region of the binding site near the solvent front. Co-crystal structure analysis indicated that several polar carbonyls, including the carboxyl side chain of D1203, resided near the solvent front and were proximal to the R³ tail aromatic ring (Figure 4). Two designs (Table 4) introduced an alcohol in the R³ group to form a hydrogen-bond interaction with this side chain. Alcohol **7h** showed higher lipophilic efficiency than **7g**. The increase in both potency and lipophilic efficiency of **7h** was derived from a hydrogen-bonding interaction with the D1203 side chain. A similar H-bond is not likely achievable by para-substituted alcohol **7g** since the ring size and substitution vectors are not suitable. Structural data confirmed a close contact between the tertiary alcohol of **7h** and the D1203 side-chain acid carbonyl (Figure 5).

In addition, the co-crystal structure of **7h** (Figure 5) showed the thiazole aromatic ring of **7h** was rotated about 30° from the plane of the 2-aminopyridine hinge-binding moiety. This conformation presented the R³ aryl ring at a suitable angle and distance to form a CH donor–π interaction with G1202.²³ Dihedral angles over 45° created a bump with the protein. Although it is very challenging to isolate the impact of the electron-richness of the aromatic to the CH–π interaction, trends highlight the general decrease in LipE with reduced electronic density of the aromatics. For example, enzymatic LipE decreased about 0.4 units from pyridine to pyrimidine analogues (**7e** and **7f** in Table 4).

Conformational analysis was carried out on compounds in Table 4. The computed energies of various conformers rotated

Table 4. Potency, ADME, and Efficiency of R³ Substitution

Compound	R ³	L1196M Ki (nM)	L1196M Cell IC ₅₀ (nM)	log D ^a	HLM Cl _{int, app} (ml/min/kg) ^b	RRCK P _{app} (A to B) (10 ⁻⁶ cm/s) ^c	LipE ^d (Ki)
6d		2.6	60	3.3	46	21	5.3
7a		2.6	176	3.4	68	27	5.2
7b		2.8	105	3.3	22	18	5.2
7c		7.5	677	3.3	17	22	4.8
7d		70	2650	2.4	3	24	4.7
7e		1.3	256	3.7	38	14	5.1
7f		15	772	3.1	49	22	4.7
7g		6.1	325	3.6	49	14	4.6
7h		0.4	27	3.6	23	18	5.8
7i		190	--	2.4	80	21	4.3

^aLog D was measured at pH 7.4.²⁰ ^bCl_{int, app} refers to the total intrinsic clearance obtained from scaling in vitro half-lives in human liver microsomes.²¹

^cRRCK cells with low transporter activity were isolated from Madin–Darby kidney cells and were used to estimate intrinsic absorptive permeability.²² ^dLipE = −log K_i − log D.

about the aryl–aryl bond (Figure 6) show that compounds able to adopt a 30° conformation with small energetic penalty tend to provide the tightest binding affinity and efficiency. For example, 7i has a 1.3 kcal/mol strain energy to adopt a protein-preferred ~30° torsion angle. This is partly reflected in a 25-fold potency

loss and a half-unit LipE decrease for 7i compared to similar compounds such as 7c.

With potent inhibitor 7h (L1196M cell IC₅₀ = 27 nM, log D = 3.6) in hand, the design focused on the thiadiazole modification to improve overall ADME properties. Compounds with lower

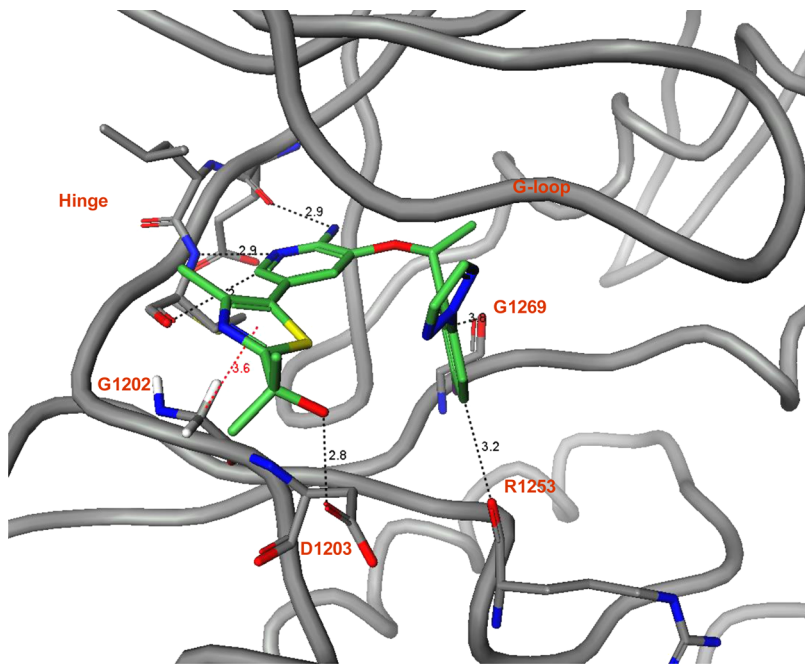


Figure 5. Co-crystal structure of **7h** and ALK wt protein (PDB 4ccu).

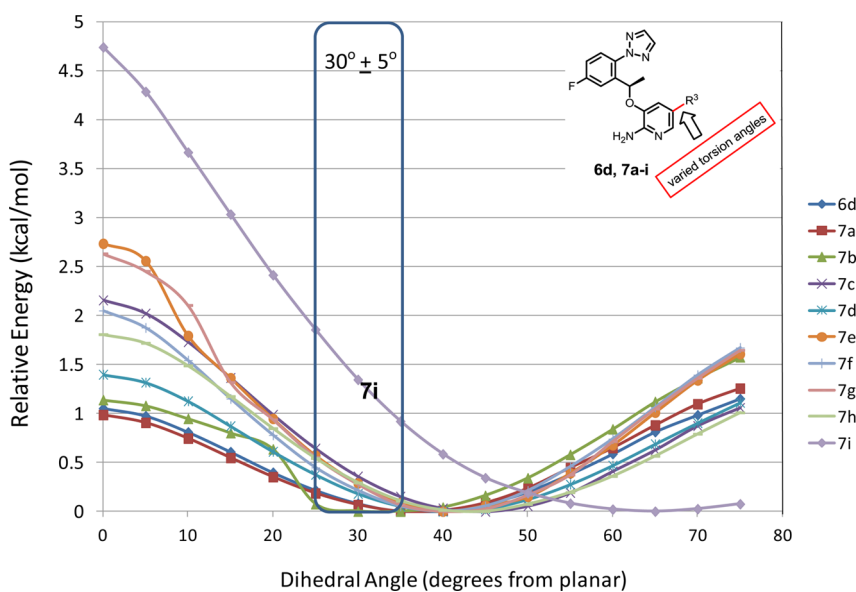


Figure 6. Relative energy profile for the torsion angle between the aminopyridine core and the R³ aryl ring for **6d** and **7a–7i** as calculated by the density functional theory (DFT) B3LYP/6-31g** method in Jaguar.

log *D* than **7h** are summarized in Table 5. Because many analogues containing thiazole groups were reaching the lower limit of the enzymatic assay, in addition to enzymatic LipE, cell LipE was also reported in Table 5. The cyclization of geminal dimethyl groups to a four-membered azetidine lowered log *D* to 2.6 due to the introduction of a basic amine (**8a**), but it had inferior cell potency and higher microsomal clearance compared with **7h**. Although **8b** lowered the lipophilicity slightly compared with **7h**, the specific structural feature yielded high *in vitro* clearance. The introduction of a sulfone motif decreased log *D* from 3.6 (**7h**) to 3.2 (**8c**), while maintaining similar cell potency, and resulted in cell LipE improvement from 4.0 (**7h**) to 4.5 (**8c**). In addition, **8c** displayed good microsomal stability and RRCK permeability.

The bound structure of **7h** with the ALK kinase domain (Figure 5) showed one methyl of the 2-propanol to be proximal to the NH of D1203 (4.2 Å). Furthermore, this NH is unsatisfied with no discernible interactions with water, ligand, or protein. Modeling suggested the addition of a hydroxyl group to this methyl could satisfy the NH as an acceptor while donating to either the carboxyl side chain of D1203 or a water molecule stabilized by the carbonyls of G1201 and D1203. Gratifyingly, the cellular potency of **8e** improved to 6.6 nM with a cellular lipophilic efficiency of 5.3, providing a highly efficient neutral ligand. Indeed, **8e** bound (Figure 7) with the tertiary OH group forming a hydrogen bond with D1203 and the primary alcohol forming hydrogen bonds with the amino group of D1203 (2.8 Å)

Table 5. Potency, ADME, and Efficiency of Substituted Thiazoles

8a-e

Compound	R ^s	L1196M Ki (nM)	L1196M Cell IC ₅₀ (nM)	log D ^a	HLM Cl _{int, app} (ml/min/kg) ^b	RRCK P _{app} (A to B) (10 ⁻⁶ cm/s) ^c	LipE ^d (Ki)	LipE ^e (cell)
7h		0.4	27	3.6	23	18	5.8	4.0
8a		0.3	52	2.6	55	3.4	6.9	4.6
8b ^g		0.6	58	3.3	138	21	5.9	3.9
8c ^g		2.6	19	3.2	13	14	5.4	4.5
8d		1.1	55	2.9	15	17	6.1	4.4
8e		0.2	6.6	2.9	15	19	6.8	5.3

^aLog D was measured at pH 7.4.²⁰ ^bCl_{int, app} refers to the total intrinsic clearance obtained from scaling in vitro half-lives in human liver microsomes.²¹ ^cRRCK cells with low transporter activity were isolated from Madin–Darby kidney cells and were used to estimate intrinsic absorptive permeability.²² ^dLipE = −log K_i − log D. ^eLipE = −log IC₅₀ − log D. ^gWhile 8b and 8c are the more potent enantiomers, the absolute chirality at the R^s substitution is undefined.

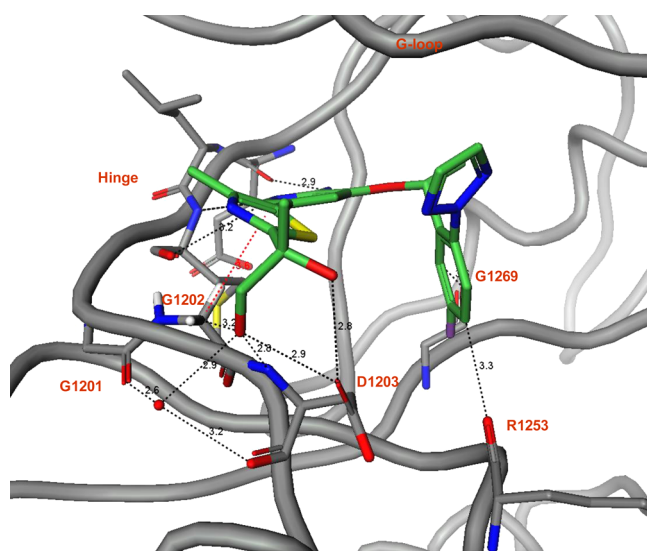


Figure 7. Co-crystal structure of 8e and ALK L1196M protein (PDB 4cd0).

and the dicarbonyl stabilized water (2.9 Å). The distance to the carboxyl group of D1203 is 2.9 Å.

Importantly, introduction of the OH group reduces lipophilicity (8e log D = 2.9) while maintaining similar RRCK P_{app} AB compared to 7h. Presumably, masking of the additional hydrogen-bond donor through an intramolecular hydrogen bond is a key contributor to maintaining permeability. Consistent with our modeling, the enantiomer (8d) resulting from introduction of a hydroxy functionality at the other carbon has eroded lipophilic efficiency.

Activity against Other ALK Mutations and in Vivo Data for 8e. On the basis of improved L1196M mutant potency, lipophilic efficiency, and balanced physicochemical properties, 8e emerged as a candidate for broader profiling in wild-type and mutant ALK driven cell lines and kinase counterscreen assays. As shown in Table 6, 8e significantly improved cell potency against ALK wt and ALK clinical mutations compared with crizotinib (1). In the engineered wt 3T3-EML4-ALK phosphorylation assay, the potency of 8e has been improved 100-fold (from 80 nM for 1 to 0.8 nM for 8e). Across the clinically identified ALK mutants in the engineered cell lines, 8e showed 67–825-fold potency increases compared to crizotinib (1). The potency gains measured by inhibition of ALK phosphorylation were consistent with the significantly improved antiproliferative potency of 8e relative to crizotinib (1) in both wild-type cell lines (parental

Table 6. Cell-Based Potency of Crizotinib (1) and 8e

	ALK phospho in 3T3-EML4-ALK engineered cells (IC_{50} , nM)								ALK-fusion-driven cell proliferation (IC_{50} , nM)				
	wt	L1196M	G1269A	S1206Y	C1156Y	F1174L	L1152R	1151Tins	H3122	H2228	Karpas299	H3122-L1196M	H3122-G1269A
crizotinib (1)	80	843	605	626	478	165	1026	3039	108	118	62	838	623
8e	0.8	6.6	9.0	4.5	0.6	0.2	3.5	24	1.3	0.8	1.7	21	24
\times -fold change	100	128	67	139	797	825	293	127	83	148	36	40	26

Table 7. Invitrogen Enzymatic IC_{50} Values of Kinases Showing the Most Sensitivity toward 8e^a

	ALK L1196M	ROS1	FER	LTK	NTRK2 (TrkB)	FES	JAK2	PTK2B (FAK2)	TNK2 (ACK)	PTK2 (FAK)	NTRK1 (TrkA)	NTRK3 (TrkC)
IC_{50} (nM)	0.2 ^b	0.02 ^b	2	2	4	5	12	12	15	16	17	18

^aInvitrogen enzyme IC_{50} using K_m levels of ATP except where noted differently. $K_i = \sim IC_{50}/2$ from the Cheng–Prusoff equation, $K_i = IC_{50}/(1 + [ATP]/K_m)$, for competitive inhibition. ^b K_i values calculated from tight-binding (Morrison) equation for competitive inhibitors tested in a Pfizer mobility shift assay.

H3122, H2228, and Karpas299) and engineered mutant lines (H3122-L1196M and H3122-G1269A).

While it was extremely potent against wt and mutant ALK, 8e also showed good kinase selectivity. Against a diverse panel of 207 kinases tested at Invitrogen, 33 off-target kinases were reported with >80% inhibition at a 1 μ M dose and further evaluated by the enzyme IC_{50} . The measured Invitrogen enzyme IC_{50} values for the kinases that showed the most sensitivity toward 8e are summarized in Table 7. In addition, 8e is very potent against ROS1 with $K_i = 0.02$ nM (in-house data).²⁴ See Supporting Information for further details of biochemical kinase selectivity of 8e.

Preclinical pharmacokinetic (PK) data was obtained on 8e to assess rat clearance, volume of distribution, half-life, and bioavailability (Table 8). The compound demonstrated 86%

Table 8. Rat Pharmacokinetic Profile of 8e^a

	intravenous	per os (oral)
dose (mg/kg)	1.0	5.0
AUC (h·nM)	667	2869
CL (mL·min ⁻¹ ·kg ⁻¹)	54	
$V_{d,ss}$ (L/kg)	2.0	
C_{max} (nM)		568
T_{max} (h)		1.3
$t_{1/2}$ (h)	0.9	
F (%)		86

^aFormulated in a solution of 10% EtOH, 40% PEG200, and 50% water. AUC, area under curve; CL, clearance; $V_{d,ss}$, steady-state volume of distribution

bioavailability in the rat. Moderate-to-high in vivo rat plasma clearance with moderate volume of distribution provided about a 1 h half-life in rat.

To evaluate the antitumor efficacy of 8e, a mouse tumor xenograft study was performed. Dosing started from day 15 post-cell implantation with tumor size around 250 mm³. As illustrated in Figure 8, 8e demonstrated dose-responsive tumor growth inhibitory activity in the NCI H3122 cell line engineered to harbor the L1196M mutation. It showed tumor stasis (100% TGI) at both the 30 mg/kg q.d. and 15 mg/kg b.i.d. doses. The highest dose (50 mg/kg b.i.d.) showed significant tumor growth regression (56%) on day 27. No significant body weight reduction was observed throughout the course of the study. The corresponding twice-daily dose PK of 8e in the last day of the TGI experiment (day 29) are shown in Figure 9.

■ CHEMISTRY

Compounds 6a–c were synthesized as outlined in Scheme 1. The starting alcohols 9, which were either commercially available or prepared according to literature procedures, underwent a Mitsunobu reaction with 5-bromo-3-hydroxy-2-nitropyridine to afford intermediates 10. For the cases in which X = OMe or F, the alcohols 9 were prepared in an enantiopure form by a diisopinocampheyl chloroborane (DIP-Cl)-mediated acetophenone reduction.²⁵ The nitro group was reduced by heating with iron powder in a mixture of AcOH and EtOH to afford amines 11. Conventional Suzuki coupling of 11 with the boronate ester of the pyrazole afforded compounds 6a–c directly. For the racemic final analogue (X = CN), the enantiomers were resolved by chiral supercritical fluid chromatography (SFC).

A reliable and scalable route was developed to access the key boronate ester 17 in an enantiopure form. Compound 17, featuring the optimized triazole headpiece, was utilized to synthesize the remainder of the analogues reported herein (6d, 7a–i, and 8a–e) through Suzuki coupling reaction or Ullman coupling (Scheme 2). The commercially available ketone 12 was reacted with triazole in the presence of Cs₂CO₃ to generate 13. Chiral reduction of 13 by use of (−)-DIP-Cl led to the formation of (S)-14 in 96% enantiomeric excess (ee). Activation of the alcohol through formation of methanesulfonate ester 15, followed by S_N2 displacement with 2-amino-5-bromo-3-hydroxypyridine in the presence of Cs₂CO₃, generated 16 in 56% yield over two steps. Gratifyingly, the S_N2 process proceeded with clean inversion, and no racemization was observed. The subsequent Pd-catalyzed borylation afforded boronate ester 17. For the initial analogues, either the boronate ester of the aryl substituent was commercially accessible and this was coupled with 16 in a fashion analogous to Scheme 1, or boronate ester 17 was generated in situ and used directly in the Suzuki coupling process with the aryl halide. In order to optimize and expedite the chemistry, a workup protocol was developed to enable isolation of 17 as a colorless solid. With bulk quantities of 17 in hand, reaction screening provided optimal Suzuki coupling conditions, which were utilized in reactions with the corresponding aryl halides (tail groups) to afford the desired final compounds (Scheme 2). Exceptionally, 7i was formed by Ullman coupling of aryl bromide 16 with 2-methylimidazole.

The majority of aryl halides used for the final Suzuki reaction are commercially available or could be readily accessed through standard literature procedures except for those thiazolo halides. A general synthetic route to access the thiazolo halides is outlined

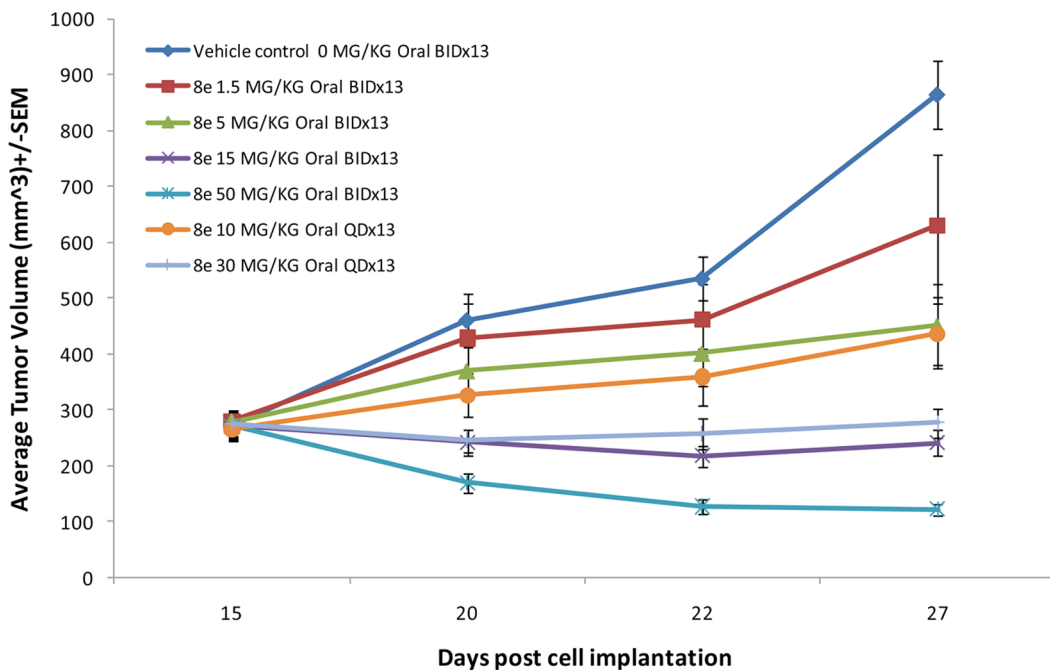


Figure 8. Dose–response curve of **8e** in H3122^{L1196M} xenografts in athymic mice.

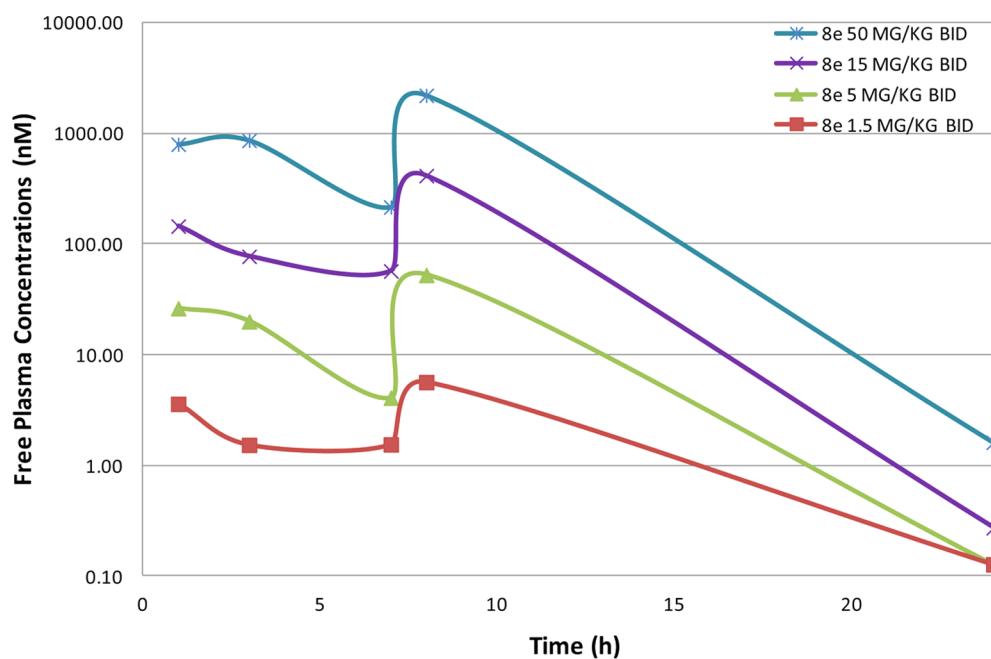
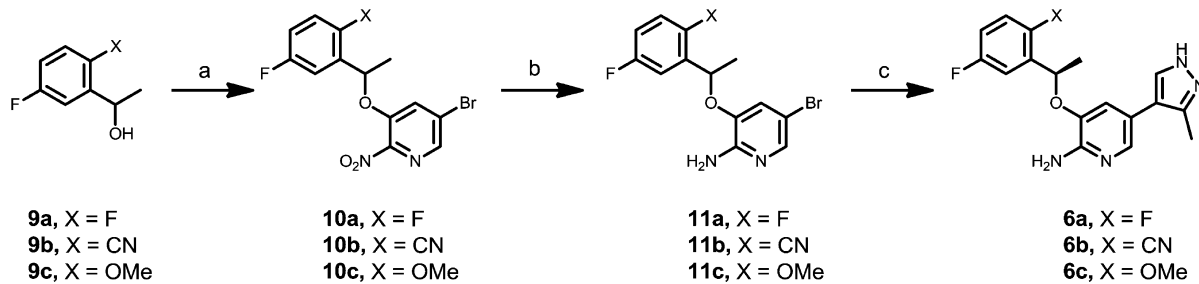


Figure 9. Twice-daily dose PK of **8e** from last day of TGI experiment (day 29) in H3122-L1196M xenografts in athymic mice.

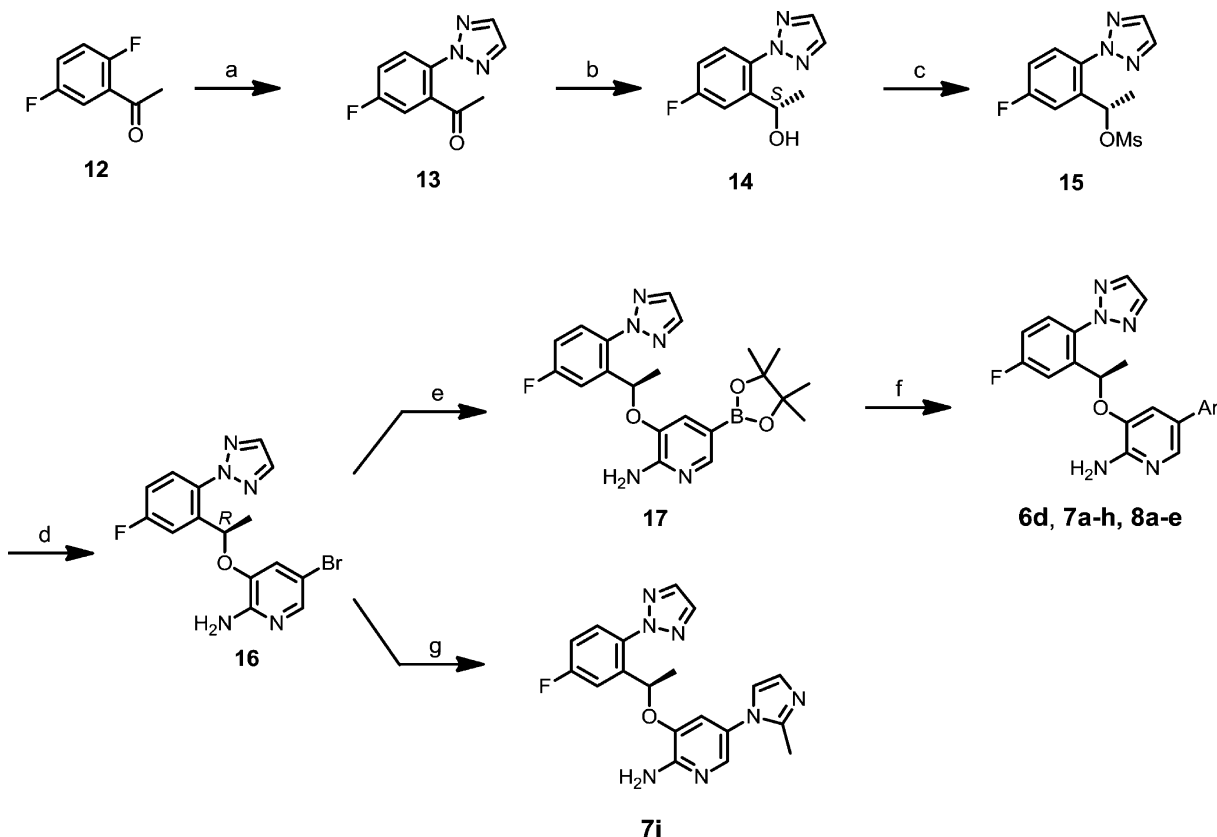
in Scheme 3. Treatment of 4-methylthiazole (**18**) with *n*-BuLi followed by subsequent trapping of the anion with a range of ketones generated tertiary alcohols **19a** and **19b**. For a range of substrates, bromination afforded the desired thiazolo bromides **20–23** for Suzuki coupling. For thiazoles featuring the diol motif, elimination of the alcohol under acidic conditions from **20** provided 1,1-disubstituted olefin **24**, which was a suitable substrate for Sharpless asymmetric dihydroxylation.²⁶ Use of either AD-mix- α or AD-mix- β provided both diol enantiomers **25** and **26** (80–85% ee, >98% ee after recrystallization), which could be utilized in Suzuki coupling to afford **8d** and **8e**, respectively.

CONCLUSIONS

The co-crystal structure of crizotinib (**1**) in the ALK kinase domain provided a basis for design of more potent second-generation ALK inhibitors. Efforts to improve the potency and efficiency of the 3-benzylxy aminopyridine series focused on optimizing both the 2,6-dichloro-3-fluorophenyl head and pyrazolopiperidine tail groups in crizotinib (**1**). A potent and lipophilic-efficient triazolophenyl head group was identified. Successful application of both structure-based and lipophilic-efficiency-focused design on the tail group optimization led to **8e**, which was potent across a broad panel of engineered ALK mutant cell lines. In addition, **8e** showed a suitable preclinical PK

Scheme 1. General Synthesis of 6a–c from Alcohol 9^a

^aReagents and conditions: (a) 1.1 equiv of Ph₃P, 1.1 equiv of 5-bromo-3-hydroxy-2-nitropyridine, 1.1 equiv of DIAD, toluene, 0 °C, 18 h. (b) 5 equiv of Fe, dioxane/AcOH (4:1), 40 °C reflux, 0.5 h. (c) 2 equiv of pyrazole boronate ester, 0.1 equiv of Pd(PPh₃)₄, 2 equiv of NaHCO₃, dioxane/water (2.5/1), 110 °C, 1.5 h.

Scheme 2. Synthesis of 6d, 7a–i, and 8a–e from Ketone 12^a

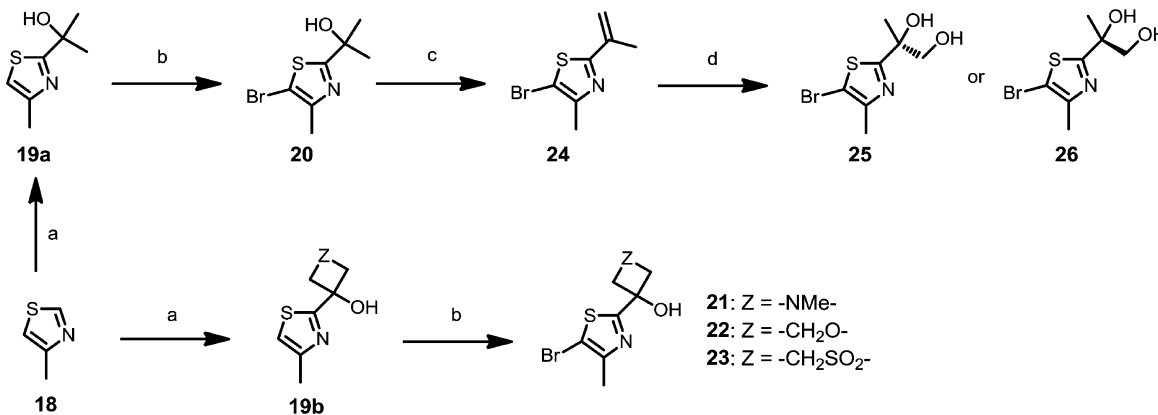
^aReagents and conditions: (a) 1.5 equiv of triazole, 1.0 equiv of Cs₂CO₃, NMP, 140 °C, 3 h, 35%. (b) 1.25 equiv of (−)-DIP-Cl, THF, −35 °C for 3 h and then rt for 18 h; 2.7 equiv of diethanolamine, TBME, rt reflux, 2 h, 99%, 96% ee. (c) 1.2 equiv of MsCl, 1.5 equiv of Et₃N, TBME, −10 °C to rt, 17 h. (d) 1.2 equiv of 2-amino-5-bromo-3-hydroxypyridine, 1.2 equiv of Cs₂CO₃, acetone, 60 °C, 16 h, 56% over two steps. (e) 1.7 equiv of bis(pinacolato)diboron, Pd(dppf)Cl₂ (5 mol %), 3.5 equiv of KOAc, DMSO, 80 °C, 3 h, 77%. (f) 1.5 equiv of ArBr, 0.05 equiv of Pd(dppf)Cl₂, 3.0 equiv of K₂CO₃, DME/water (5:1), 120 °C microwave, 1 h; or 1.5 equiv of ArBr, 0.05 equiv of Pd(dppf)Cl₂, 2.5 equiv of CsF, MeOH, 120 °C microwave, 1 h; or 1.3 equiv of ArBr, 0.05 equiv of Pd-132, 3 equiv of CsF, MeOH, 50 °C, 1 h. (g) 5 equiv of methylimidazole, 1.5 equiv of CuI, 3 equiv of Cs₂CO₃, NMP, 150 °C, microwave, 5 h, 2%.

profile and demonstrated robust tumor growth inhibition in a crizotinib-resistant (H3122-L1196M) *in vivo* model.

EXPERIMENTAL METHODS

Starting materials and other reagents were purchased from commercial suppliers and were used without further purification unless otherwise indicated. Compound 8e, also known as PF-06439015, is now commercially available from Sigma Aldrich. All reactions were performed under a positive pressure of nitrogen or argon or with a drying tube, at ambient temperature (unless otherwise stated), in

anhydrous solvents, unless otherwise indicated. Analytical thin-layer chromatography was performed on glass-backed silica gel 60 F 254 plates [Analtech (0.25 mm)] and eluted with the appropriate solvent ratios (v/v). The reactions were assayed by high-performance liquid chromatography (HPLC) or thin-layer chromatography (TLC) and terminated as judged by the consumption of starting material. The TLC plates were visualized by UV, phosphomolybdic acid stain, or iodine stain. Microwave-assisted reactions were run in a Biotage Initiator. ¹H NMR spectra were recorded on a Bruker instrument operating at 400 MHz unless otherwise indicated. ¹H NMR spectra are obtained as DMSO-d₆ or CDCl₃ solutions as indicated (reported in parts per

Scheme 3. General Synthesis of Thiazole Halides as Precursors for Suzuki Coupling Reactions^a

^aReagents and conditions: (a) 1.0 equiv of ketone, 1.0 equiv of *n*-BuLi, THF, −78 °C, 0.5 h. (b) 1.0 equiv of NBS, DMF 0 °C, overnight. (c) 1.1 equiv of H₂SO₄, AcOH, 80–85 °C, 20 h. (d) AD-mix- α or - β , THF/*t*-BuOH/H₂O (1:1:1), 25 °C, 60 h.

million, ppm), with chloroform as the reference standard (7.25 ppm) or DMSO-*d*₆ (2.50 ppm). Other NMR solvents were used as needed. When peak multiplicities are reported, the following abbreviations are used: s = singlet, d = doublet, t = triplet, m = multiplet, br = broadened, dd = doublet of doublets, dt = doublet of triplets. Coupling constants, when given, are reported in hertz. Mass spectra were obtained via liquid chromatography–mass spectrometry (LC-MS) on an Agilent instrument with atmospheric pressure chemical ionization (APCI) or electrospray ionization (ESI). High-resolution mass measurements were carried out on an Agilent TOF 6200 series with ESI. All test compounds showed >95% purity as determined by combustion analysis or by HPLC. HPLC conditions were as follows: XBridge C18 column @ 80 °C, 4.6 mm × 150 mm, 5 μm, 5%/95% MeOH/H₂O buffered with 0.2% formic acid/0.4% ammonium formate, 3 min run, flow rate 1.2 mL/min, UV detection (λ = 254, 224 nm). Combustion analyses were performed by Atlantic Microlab, Inc. (Norcross, GA).

3-[(*R*)-1-(2-Chloro-5-fluorophenyl)ethoxy]-5-[1-(piperidin-4-yl)-1*H*-pyrazol-4-yl]pyridin-2-amine (1a). For the synthetic approach to 1a, see ref 11c. LC-MS (APCI) *m/z* 417 (M + H)⁺; ¹H NMR (700 MHz, DMSO-*d*₆) δ 7.95 (s, 1H), 7.75 (s, 1H), 7.59 (s, 1H), 7.54–7.58 (m, 1H), 7.51 (dd, *J* = 8.80, 4.84 Hz, 1H), 7.17 (td, *J* = 8.20, 2.97 Hz, 1H), 7.03 (s, 1H), 5.84 (s, 2H), 5.83–5.79 (m, 1H), 4.17–4.09 (m, 1H), 3.02 (d, *J* = 12.10 Hz, 2H), 2.56 (t, *J* = 11.77 Hz, 2H), 1.92 (d, *J* = 10.56 Hz, 2H), 1.76 (br s, 2H), 1.59 (d, *J* = 6.16 Hz, 3H), one NH proton is missing due to deuterium exchange.

(*R*)-5-Bromo-3-[1-(2,5-difluorophenyl)ethoxy]-2-nitropyridine (10a). To an ice-cooled solution (0 °C) of (*S*)-1-(5-fluoro-2-methoxyphenyl)ethanol^{25b} (99. 5% ee, 10.0 g, 63.2 mmol) and triphenylphosphine (19.1 g, 72.7 mmol) in toluene (400 mL) was added a solution of 5-bromo-3-hydroxy-2-nitropyridine (14.5 g, 66.4 mmol) in toluene (100 mL), followed by diisopropyl azodicarboxylate (14.8 g, 73 mmol) at such a rate as to maintain the temperature below 10 °C. The resulting mixture was stirred at room temperature for 18 h. The crude reaction mixture was concentrated and 100 mL of fresh toluene was added. The yellow solution was stirred at −78 °C for 90 min, after which the precipitate was filtered off and washed with precooled toluene (3 × 75 mL). The filtrate was concentrated under reduced pressure and fresh toluene was added (150 mL). The solution was washed with 1 M NaOH (75 mL) to remove excess hydroxypyridine and then dried over magnesium sulfate, filtered, and evaporated to give a yellow gum. The crude material was purified by column chromatography on silica gel, eluted with 3/1 heptane/EtOAc, to give the desired product 10a (21.03 g, 93% yield) as a yellow oil. LC-MS (APCI) *m/z* 359 (M + H)⁺; ¹H NMR (400 MHz, CDCl₃) δ 8.12 (d, *J* = 1.6 Hz, 1H), 7.48 (d, *J* = 2 Hz, 1H), 7.17 (ddd, *J* = 8.5, 5.6, 3.1 Hz, 1H), 7.11–7.06 (m, 1H), 7.02–6.98 (m, 1H), 5.75 (q, *J* = 6.4 Hz, 1H), 1.71 (d, *J* = 6.2 Hz, 3H).

(*R*)-5-Bromo-3-[1-(2,5-difluorophenyl)ethoxy]pyridin-2-amine (11a). To a solution of 10a (21.0 g, 46 mmol) in dioxane (200 mL), was added glacial AcOH (26 mL) at room temperature. The

solution was warmed to 40 °C. At this temperature, 325 mesh iron (12.7 g) was added to the solution in a portionwise manner. After the reaction mixture was stirred at 40 °C for 30 min, another 26 mL of glacial AcOH was added. After the reaction mixture was stirred for 10 min, 2 M HCl (200 mL) was added and the solution was filtered through Celite. The remaining iron residue was washed with 2 M HCl (2 × 100 mL). The aqueous layer was extracted with *tert*-butyl methyl ether (TBME; 1 × 250 mL) and the TBME layer was back-washed with 2 M HCl (150 mL). The aqueous layer was made basic with ammonia and extracted with TBME (2 × 250 mL). The combined TBME layers were decanted off and filtered through Celite. The filtrate was dried with MgSO₄, filtered, and evaporated to give 11a (17.5 g, 91% yield) as a clear oil. This material was used without further purification in the subsequent Suzuki coupling step. LC-MS (APCI) *m/z* 329 (M + H)⁺; ¹H NMR (400 MHz, CDCl₃) δ 7.69 (d, *J* = 2 Hz, 1H), 7.11–6.95 (m, 3H), 6.85 (d, *J* = 2 Hz, 1H), 5.57 (q, *J* = 6.5 Hz, 1H), 4.90 (br s, 2H), 1.68 (d, *J* = 6.6 Hz, 3H).

(*R*)-3-[1-(2,5-Difluorophenyl)ethoxy]-5-(3-methyl-1*H*-pyrazol-4-yl)pyridin-2-amine (6a). To a suspension of 11a (100 mg, 0.3 mmol), 3-methyl-4-(4,4,5,5-tetramethyl-1,3,2-dioxaborolan-2-yl)-1*H*-pyrazole (158 mg, 0.76 mmol), and palladium tetrakis(triphenylphosphine) (35 mg, 0.03 mmol) in dioxane (12.5 mL) were added NaHCO₃ (64 mg, 0.76 mmol) and water (5 mL). The reaction mixture was thoroughly degassed. After being heated at 110 °C for 90 min, the reaction mixture was cooled to room temperature and partitioned between 10% citric acid solution (25 mL) and TBME (25 mL). The aqueous layer was made basic with ammonia and further extracted with TBME (25 mL). The organic layer was then dried with MgSO₄, filtered, and evaporated. The residue was purified by flash column chromatography over silica gel, eluted with 1/4 heptane/EtOAc followed by 100% EtOAc, to provide the desired product 6a (60 mg, 60% yield) as a clear oil. LC-MS (APCI) *m/z* 331 (M + H)⁺; ¹H NMR (400 MHz, CDCl₃) δ 7.66 (d, *J* = 2 Hz, 1H), 7.47 (s, 1H), 7.12–7.04 (m, 2H), 6.99–6.93 (m, 1H), 6.78 (d, *J* = 1.6 Hz, 1H), 5.73 (br s, 2H), 5.62 (q, *J* = 6.50 Hz, 1H), 5.12 (br s, 1H), 2.22 (s, 3H), 1.71 (d, *J* = 6.26 Hz, 3H).

2-[(1*S*)-1-[(2-Amino-5-(3-methyl-1*H*-pyrazol-4-yl)-pyridin-3-yl]oxy]ethyl]-4-fluorobenzonitrile (6b). In a similar manner to the preparation of 6a, racemic 11b (280 mg, 0.83 mmol) was reacted with 3-methyl-4-(4,4,5,5-tetramethyl-1,3,2-dioxaborolan-2-yl)-1*H*-pyrazole (433 mg, 2.08 mmol) to afford 6b (45 mg, 15% yield) as a colorless solid after chiral separation. LC-MS (ESI) *m/z* 338.04 (M + H)⁺; ¹H NMR (400 MHz, CDCl₃) δ 7.79–7.63 (m, 2H), 7.51 (s, 1H), 7.31–7.25 (m, 1H), 7.21–7.03 (m, 1H), 6.73 (d, *J* = 1.95 Hz, 1H), 5.79–5.58 (m, 1H), 4.95 (br s, 2H), 2.25 (s, 3H), 1.78 (d, *J* = 6.25 Hz, 3H), one NH proton is missing due to deuterium exchange. Chiral separation by HPLC afforded 6b with >99% ee by use of an AD-H column eluted with 50/50 MeOH/EtOH at 0.5 mL/min. Compound 6b was obtained as peak 1 (9.55 min) and the inactive enantiomer as peak 2 (13.56 min).

3-[(1*R*)-1-(5-Fluoro-2-methoxyphenyl)ethoxy]-5-(5-methyl-1*H*-pyrazol-4-yl)pyridin-2-amine (6c). In a similar manner to the

preparation of **6a**, **11c** (250 mg, 0.66 mmol) was reacted with 3-methyl-4-(4,4,5,5-tetramethyl-1,3,2-dioxaborolan-2-yl)-1*H*-pyrazole (239 mg, 1.15 mmol) to afford **6c** (128 mg, 57% yield) as a pale, dense yellow foam after purification. LC-MS (APCI) *m/z* 343 (M + H)⁺; ¹H NMR (400 MHz, methanol-*d*₄) δ 7.53–7.42 (m, 2H), 7.08 (dd, *J* = 2.73, 8.98 Hz, 1H), 7.04–6.93 (m, 2H), 6.79 (d, *J* = 1.56 Hz, 1H), 5.78 (q, *J* = 6.51 Hz, 1H), 4.89 (br s, 2H), 3.89 (s, 3H), 2.10 (s, 3H), 1.64 (d, *J* = 6.25 Hz, 3H), one NH proton is missing due to deuterium exchange.

1-(5-Fluoro-2-[1,2,3-triazol-2-yl]phenyl)ethanone (13). To a solution of 2,5-difluoroacetophenone **12** (10.0 g, 64 mmol) in 1-methyl-2-pyrrolidinone (10 mL) were added potassium carbonate (8.84 g, 64 mmol) and 1*H*-1,2,3-triazole (6.64 g, 96 mmol). The mixture was heated to 140 °C for 3 h under an atmosphere of nitrogen. The reaction was allowed to cool and then partitioned between ethyl acetate (300 mL) and aqueous ammonium chloride solution (1 M, 100 mL). The organic phase was washed with water (3 × 200 mL) and then dried over magnesium sulfate, filtered, and concentrated. The residue was purified by chromatography on silica gel, eluted with 9/1 heptane/EtOAc, to produce **13** (4.6 g, 35% yield) as a brown oil. LC-MS (APCI) *m/z* 206 (M + H)⁺; ¹H NMR (400 MHz, CDCl₃) δ 7.85–7.80 (m, 3H), 7.28–7.20 (m, 2H), 2.17 (s, 3H).

(S)-1-[5-Fluoro-2-(2H-1,2,3-triazol-2-yl)phenyl]ethanol (14). To a solution of (−)-DIP-Cl (21.3 g, 66.4 mmol) in THF (60 mL) at −35 °C was added a solution of **13** (10.9 g, 53.1 mmol) in THF (20 mL) in a dropwise manner at such a rate as to maintain the temperature below −27 °C. The resulting mixture was stirred at −35 °C for 3 h and then allowed to warm slowly to room temperature over a period of 18 h. The mixture was evaporated under reduced pressure to remove the majority of the THF. The resulting residue was dissolved in TBME (150 mL) and rapidly stirred with an overhead stirrer while diethanolamine (15.1 g, 2.7 equiv) was added, and the temperature was allowed to rise to 50 °C during the addition. The resulting mixture was stirred for 1 h before filtration. The filter cake was washed with TBME (2 × 100 mL) and discarded. The combined filtrate was evaporated under reduced pressure and the resulting crude product was purified by chromatography on silica gel, eluted with 1/1 heptane/toluene, followed by a gradient of heptane/TBME (1/1 to 0/1) to produce **14** (10.9 g, 99% yield) as a colorless oil. LC-MS (APCI) *m/z* 208 (M + H)⁺; ¹H NMR (400 MHz, CDCl₃) δ 7.86 (s, 2H), 7.59 (dd, *J* = 8.98, 5.08 Hz, 1H), 7.38 (dd, *J* = 9.57, 2.93 Hz, 1H), 7.09 (ddd, *J* = 8.79, 7.62, 3.12 Hz, 1H), 4.85 (dd, *J* = 6.64, 1.17 Hz, 1H), 1.43 (d, *J* = 6.64 Hz, 3H), one OH proton is missing due to deuterium exchange. Compound **14** was obtained in 96% ee (*S*) as determined by SFC on a Chiralpak AD-H 4.6 × 250 mm column, 10% MeOH @ 140 bar, 3 mL/min.

(S)-1-[5-Fluoro-2-(2H-1,2,3-triazol-2-yl)phenyl]ethyl Methanesulfonate (15). To a solution of **14** (15.1 g, 72.9 mmol) in TBME (150 mL) was added triethylamine (15.4 mL, 110 mmol). The solution was cooled to −20 °C, and methanesulfonyl chloride (6.72 mL, 86.8 mmol) was added as a solution in TBME (30 mL) via an addition funnel. The reaction mixture was kept at −10 °C for 1 h and then allowed to warm to room temperature. After the mixture was stirring at room temperature for 16 h, water (80 mL) was added to the reaction mixture. The organic layer was washed with saturated NaHCO₃ (80 mL) and 0.1 M HCl (2 × 80 mL), dried over Na₂SO₄, filtered, and evaporated to give **15** (17.74 g, 85% yield) as a yellow oil, which was used without further purification. LC-MS (APCI) *m/z* 286 (M + H)⁺; ¹H NMR (400 MHz, CDCl₃) δ 7.89 (s, 2H), 7.69 (dd, *J* = 9.09, 5.05 Hz, 1H), 7.43 (dd, *J* = 9.22, 2.91 Hz, 1H), 7.19 (ddd, *J* = 8.91, 7.39, 2.91 Hz, 1H), 6.16 (qd, *J* = 6.40, 1.01 Hz, 1H), 2.86 (s, 3H), 1.71 (d, *J* = 6.57 Hz, 3H). Compound **15** was obtained in 96–96.5% ee (*S*) as determined by SFC on a Chiralpak AD-H 4.6 × 250 mm column, 10% MeOH @ 140 bar, 3 mL/min.

(R)-5-Bromo-3-[1-[5-fluoro-2-(2H-1,2,3-triazol-2-yl)phenyl]ethoxy]pyridin-2-amine (16). To a suspension of cesium carbonate (24.3 g, 74.6 mmol) and 2-amino-5-bromopyridin-3-ol (14.1 g, 74.6 mmol) in acetone (100 mL) was added a solution of **15** (17.73 g, 62.1 mmol) in acetone (100 mL) via an addition funnel. After the reaction mixture was heated at 60 °C for 16 h and stirred at room temperature for a further 16 h, the reaction mixture was filtered through Celite and washed with EtOAc. The filtrate was concentrated and purified by

column chromatography on silica gel, eluted with 0–20% EtOAc/heptane, to give **16** (15 g, 67% yield) as a yellow foam. LC-MS (APCI) *m/z* 378 (M + H)⁺; ¹H NMR (400 MHz, CDCl₃) δ 7.92 (s, 2H), 7.69–7.63 (m, 2H), 7.30–7.24 (m, 1H), 7.18–7.12 (m, 1H), 6.87 (d, *J* = 1.77 Hz, 1H), 5.73 (d, *J* = 6.32 Hz, 1H), 4.73 (br s, 2H), 1.58 (s, 3H). Compound **16** was obtained in 96% ee as determined by SFC on a LUX cellulose 4.6 μm × 250 mm column, 5–45% MeOH ramping 10%/min @ 140 bar, 3 mL/min.

3-[(*R*)-1-(5-Fluoro-2-[1,2,3-triazol-2-yl]phenyl)ethoxy]-5-(4,4,5,5-tetramethyl-[1,3,2]dioxaborolan-2-yl)pyridin-2-yl-amine (17). Dimethyl sulfoxide (DMSO, 15 mL) was bubbled with argon gas for 15 min and then added to a mixture of bis(pinacolato)-diboron (B₂pin₂; 332 mg, 1.31 mmol), **16** (291 mg, 0.769 mmol), and potassium acetate (264 mg, 2.69 mmol) under argon atmosphere. 1,1'-Bis(diphenylphosphino)ferrocene-palladium(II) dichloride [Pd(dppf)-Cl₂, 31 mg, 0.038 mmol] was added to the mixture, which was further bubbled with argon gas for 5 min and then placed in an 80 °C oil bath for 3 h. After the mixture was cooled to room temperature, ethyl acetate, aqueous NaH₂PO₄ (1 M), and brine were added. The mixture was extracted three times with EtOAc, and the combined extracts were dried over Na₂SO₄, filtered, and evaporated to a black tar, which was then resuspended in EtOAc. The product was extracted into water (10 mL) containing HCl (0.8 mmol). To the product in water was added aqueous Na₂HPO₄ (0.25 M, 0.75 mmol, 3 mL). The pH was then further adjusted to ca. 5 by addition of aqueous NaH₂PO₄ (1 M). The cream-colored product precipitated, and EtOAc and brine were added. The product dissolved, and the aqueous layer was extracted with EtOAc (3 × 30 mL). The combined EtOAc extracts were dried over sodium sulfate, filtered, and evaporated to afford **17** (250 mg, 77% yield) as a cream-colored solid, which was used without further purification. LC-MS (APCI) *m/z* 426 (M + H)⁺; ¹H NMR (400 MHz, DMSO-*d*₆) δ 8.23 (s, 2H), 7.77–7.65 (m, 3H), 7.36 (dt, *J* = 8.5, 2.8 Hz, 1H), 6.72 (s, 1H), 6.70 (br s, 2H), 5.70 (q, *J* = 6.63 Hz, 1H), 1.58 (d, *J* = 6.15 Hz, 3H), 1.23 (s, 12H).

3-[(*1R*)-1-[5-Fluoro-2-(2H-1,2,3-triazol-2-yl)phenyl]ethoxy]-5-(5-methyl-1*H*-pyrazol-4-yl)pyridin-2-amine (6d). In a similar manner to the preparation of **6a**, **16** (250 mg, 0.66 mmol) was reacted with 3-methyl-4-(4,4,5,5-tetramethyl-1,3,2-dioxaborolan-2-yl)-1*H*-pyrazole (343 mg, 1.65 mmol) to afford **6d** (135 mg, 54% yield) as a white foam after purification. LC-MS (ESI) *m/z* 380.1 (M + H)⁺; ¹H NMR (400 MHz, DMSO-*d*₆) δ 8.22 (s, 2H), 7.67 (dd, *J* = 8.84, 5.05 Hz, 1H), 7.59 (dd, *J* = 9.73, 2.91 Hz, 1H), 7.53 (d, *J* = 1.77 Hz, 1H), 7.44 (br s, 1H), 7.34 (td, *J* = 8.34, 3.03 Hz, 1H), 6.60 (d, *J* = 1.52 Hz, 1H), 5.82 (s, 2H), 5.71–5.35 (m, 1H), 2.05 (s, 3H), 1.59 (d, *J* = 6.06 Hz, 3H), one NH proton is missing due to deuterium exchange.

5-(1,3-Dimethyl-1*H*-pyrazol-4-yl)-3-[(*1R*)-1-[5-fluoro-2-(2H-1,2,3-triazol-2-yl)phenyl]ethoxy]pyridin-2-amine (7a). A mixture of **16** (75 mg, 0.2 mmol), 1,3-dimethyl-4-(4,4,5,5-tetramethyl-[1,3,2]dioxaborolan-2-yl)-1*H*-pyrazole (74.8 mg, 0.34 mmol), and cesium fluoride (91.1 mg, 0.91 mmol) was taken up in methanol (2 mL), and the solution was thoroughly degassed. PdCl₂(dppf) (8.2 mg, 0.01 mmol) was added to the solution, and the reaction was heated in the microwave at 120 °C for 1 h. The reaction was allowed to cool, and the filtrate was passed through a 2 μm syringe filter prior to being purified by SFC to afford **7a** (51 mg, 66% yield) as a colorless solid. LC-MS (APCI) *m/z* 394 (M + H)⁺; ¹H NMR (600 MHz, DMSO-*d*₆) δ 8.23 (s, 2H), 7.66 (dd, *J* = 8.88, 5.10 Hz, 1H), 7.58 (dd, *J* = 9.82, 3.02 Hz, 1H), 7.54 (s, 1H), 7.48 (d, *J* = 1.51 Hz, 1H), 7.33 (td, *J* = 8.50, 3.02 Hz, 1H), 6.56 (d, *J* = 1.89 Hz, 1H), 5.86 (s, 2H), 5.53 (q, *J* = 6.29 Hz, 1H), 3.72 (s, 3H), 1.94 (s, 3H), 1.58 (d, *J* = 6.42 Hz, 3H).

4-(6-Amino-5-[(*1R*)-1-[5-fluoro-2-(2H-1,2,3-triazol-2-yl)phenyl]ethoxy]pyridin-3-yl)-1-methyl-1*H*-pyrazole-3-carbonitrile (7b). Compound **17** (500 mg, 1.18 mmol), 4-bromo-1-methyl-1*H*-pyrazole-3-carbonitrile (328 mg, 1.76 mmol), and potassium carbonate (488 mg, 3.53 mmol) were all added to a microwave vial, followed by the addition of dimethyl ether (DME; 10 mL) and water (2 mL). The mixture was thoroughly degassed, and Pd(dppf)Cl₂ (48.2 mg, 0.059 mmol) was added. The reaction was heated in the microwave at 120 °C for 1 h. The reaction was partitioned between EtOAc and water. The organic layers were separated, dried over Na₂SO₄, and evaporated to

give a residue, which was purified by reverse-phase HPLC to provide **7b** (139 mg, 29% yield) as a white solid. LC-MS (APCI) *m/z* 405 (M + H)⁺; ¹H NMR (400 MHz, DMSO-*d*₆) δ 8.22 (s, 2H), 7.98 (s, 1H), 7.73 (d, *J* = 2.02 Hz, 1H), 7.69 (dd, *J* = 9.73, 2.91 Hz, 1H), 7.62 (dd, *J* = 8.84, 5.05 Hz, 1H), 7.32 (td, *J* = 8.40, 2.91 Hz, 1H), 6.81 (d, *J* = 1.52 Hz, 1H), 6.20 (s, 2H), 5.56 (q, *J* = 6.32 Hz, 1H), 3.94 (s, 3H), 1.57 (d, *J* = 6.32 Hz, 3H).

3-[(1*R*)-1-[5-Fluoro-2-(2*H*-1,2,3-triazol-2-yl)phenyl]ethoxy]-5-(1-methyl-1*H*-pyrazol-5-yl)pyridin-2-amine (7c**).** In a similar manner to the preparation of **6a**, **16** (200 mg, 0.53 mmol) was reacted with 1-methyl-5-(4,4,5,5-tetramethyl-1,3,2-dioxaborolan-2-yl)-1*H*-pyrazole (220 mg, 1.06 mmol) to afford **7c** (168 mg, 84% yield) as a white solid after purification. LC-MS (APCI) *m/z* 379.1 (M + H)⁺; ¹H NMR (400 MHz, CDCl₃) δ 7.87 (s, 2H), 7.71 (d, *J* = 1.6 Hz, 1H), 7.62 (dd, *J* = 8.8, 4.9 Hz, 1H), 7.44 (d, *J* = 2 Hz, 1H), 7.29 (dd, *J* = 6.2, 3.1 Hz, 1H), 7.12 (ddd, *J* = 8.8, 7.4, 2.9 Hz, 1H), 6.80 (d, *J* = 1.6 Hz, 1H), 6.16 (d, *J* = 2 Hz, 1H), 5.78 (dd, *J* = 6.2, 1.2 Hz, 1H), 4.92 (br s, 2H), 3.67 (s, 3H), 1.61 (d, *J* = 6.2 Hz, 3H).

3-[(1*R*)-1-[5-Fluoro-2-(2*H*-1,2,3-triazol-2-yl)phenyl]ethoxy]-5-(1-methyl-1*H*-1,2,3-triazol-5-yl)pyridin-2-amine (7d**).** In a similar manner to the preparation of **6a**, **17** (263 mg, 0.64 mmol) was reacted with 1-methyl-5-iodotriazole (134 mg, 0.64 mmol) to afford **7d** (63 mg, 26% yield) as a white foam after purification. LC-MS (ESI) *m/z* 381 (M + H)⁺; ¹H NMR (400 MHz, CDCl₃) δ 7.89 (s, 2H), 7.70 (d, *J* = 1.56 Hz, 1H), 7.62–7.59 (m, 1H), 7.60 (s, 1H), 7.29–7.26 (m, 1H), 7.14–7.11 (m, 1H), 6.80 (d, *J* = 1.95 Hz, 1H), 5.71 (q, *J* = 6.2 Hz, 1H), 5.22 (br s, 2H), 3.86 (s, 3H), 1.62 (d, *J* = 6.25 Hz, 3H).

5-[(1*R*)-1-[5-Fluoro-2-(2*H*-1,2,3-triazol-2-yl)phenyl]ethoxy]-2'-methoxy-3,3'-bipyridin-6-amine (7e**).** In a similar manner to the preparation of **7a**, **16** (50 mg, 0.13 mmol) was reacted with 2-methoxy-3-pyridineboronic acid (54.9 mg, 0.26 mmol) to afford **7e** (29 mg, 54% yield) as a white solid after purification. LC-MS (ESI) *m/z* 407.1 (M + H)⁺; ¹H NMR (400 MHz, DMSO-*d*₆) δ 8.18 (s, 2H), 8.05 (dd, *J* = 4.93, 1.64 Hz, 1H), 7.70–7.59 (m, 3H), 7.53 (dd, *J* = 7.33, 1.52 Hz, 1H), 7.34 (td, *J* = 8.34, 3.03 Hz, 1H), 7.00 (dd, *J* = 7.33, 5.05 Hz, 1H), 6.81 (d, *J* = 1.26 Hz, 1H), 6.08 (s, 2H), 5.59 (q, *J* = 5.73 Hz, 1H), 3.70 (s, 3H), 1.59 (d, *J* = 5.73 Hz, 3H).

3-[(1*R*)-1-[5-Fluoro-2-(2*H*-1,2,3-triazol-2-yl)phenyl]ethoxy]-5-(4-methoxypyrimidin-5-yl)pyridin-2-amine (7f**).** In a similar manner to the preparation of **6a**, **16** (150 mg, 0.40 mmol) was reacted with 4-methoxy-5-pyrimidineboronic acid (84 mg, 0.55 mmol) to afford **7f** (32 mg, 20% yield) as a white solid after purification. LC-MS (APCI) *m/z* 408.1 (M + H)⁺; ¹H NMR (400 MHz, CDCl₃) δ 8.71 (s, 1H), 8.35 (s, 1H), 7.89 (s, 2H), 7.80 (d, *J* = 1.6 Hz, 1H), 7.64 (dd, *J* = 8.8, 4.9 Hz, 1H), 7.28–7.23 (m, 2H), 7.18–7.13 (m, 1H), 6.44 (br s, 2H), 5.84 (q, *J* = 6.04 Hz, 1H), 3.92 (s, 3H), 1.65 (d, *J* = 6.6 Hz, 3H).

2-(6'-Amino-5'-(1*R*)-1-[5-fluoro-2-(2*H*-1,2,3-triazol-2-yl)phenyl]ethoxy)-2-methyl-3,3'-bipyridin-6-yl)propan-2-ol (7g**).** Compound **16** (100 mg, 0.26 mmol), B₂Pi_n (114 mg, 0.45 mmol), KOAc (91 mg, 0.92 mmol), and Pd(dppf)Cl₂ (9.5 mg, 0.01 mmol) were combined in a microwave vial, and DMSO (1 mL) was added. The mixture was thoroughly degassed and heated in the microwave at 80 °C for 3 h. LC-MS indicated that all **16** had been consumed, and the intermediate boronate ester **17** could be observed. 2-(5-Bromo-6-methylpyridin-2-yl)propan-2-ol (91 mg, 0.40 mmol), cesium fluoride (120 mg, 0.79 mmol), Pd(dppf)Cl₂ (9.5 mg, 0.01 mmol), and methanol (2 mL) were all added to the vial, which was heated in the microwave at 120 °C for 1 h. The reaction was partitioned between EtOAc and saturated aqueous NaHCO₃. The organic layers were separated, dried over Na₂SO₄, and evaporated to give a residue, which was purified by reverse-phase HPLC to provide **7g** (56 mg, 47% yield) as a white solid. LC-MS (APCI) *m/z* 449.1 (M + H)⁺; ¹H NMR (600 MHz, DMSO-*d*₆) δ 8.15 (s, 2H), 7.67–7.58 (m, 2H), 7.48–7.42 (m, 2H), 7.39 (d, *J* = 8.31 Hz, 1H), 7.35 (s, 1H), 6.59 (d, *J* = 1.51 Hz, 1H), 6.06 (s, 2H), 5.56 (d, *J* = 6.04 Hz, 1H), 5.24–5.15 (m, 1H), 2.15 (s, 3H), 1.58 (d, *J* = 6.42 Hz, 3H), 1.42 (s, 6H).

2-[5-(6-Amino-5-[(1*R*)-1-[5-fluoro-2-(2*H*-1,2,3-triazol-2-yl)phenyl]ethoxy]pyridin-3-yl)-4-methyl-1,3-thiazol-2-yl]propan-2-ol (7h**).** Compound **17** (112 mg, 0.26 mmol), 2-(5-bromo-4-methylthiazol-2-yl)propan-2-ol (92 mg, 0.39 mmol), and cesium

fluoride (139 mg, 0.91 mmol) were all added to a microwave vial, and methanol (4 mL) was added. The mixture was thoroughly degassed, and Pd(dppf)Cl₂ (10.6 mg, 0.01 mmol) was added. The reaction was heated in the microwave at 120 °C for 1 h. The reaction was partitioned between EtOAc and water. The organic layers were separated, dried over Na₂SO₄, and evaporated to give a residue, which was purified by reverse-phase HPLC to provide **7h** (30 mg, 25% yield) as a tan powder. LC-MS (APCI) *m/z* 455 (M + H)⁺; ¹H NMR (400 MHz, DMSO-*d*₆) δ 8.19 (s, 2H), 7.67 (dd, *J* = 8.72, 5.18 Hz, 1H), 7.61 (dd, *J* = 9.60, 2.78 Hz, 1H), 7.52 (d, *J* = 1.77 Hz, 1H), 7.39–7.31 (m, 1H), 6.63 (s, 1H), 6.17 (br s, 2H), 5.84 (s, 1H), 5.66–5.56 (m, 1H), 2.06 (s, 3H), 1.58 (d, *J* = 6.32 Hz, 3H), 1.47 (s, 6H).

3-[(R)-1-(5-Fluoro-2-[1,2,3]triazol-2-ylphenyl)ethoxy]-5-(2-methylimidazol-1-yl)pyridin-2-ylamine (7i**).** A mixture of **16** (50 mg, 0.13 mmol), 2-methylimidazole (54.2 mg, 0.66 mmol), Cs₂CO₃ (129 mg, 0.4 mmol), and CuI (37.7 mg, 0.2 mmol) in *N*-methyl-2-pyrrolidone (NMP; 0.44 mL) was degassed, purged with nitrogen, and heated to 150 °C in the microwave. After 5 h, the crude reaction mixture was poured into water (100 mL) and extracted with TBME (2 × 50 mL). The combined organic extracts were washed with water and brine, dried over MgSO₄, filtered, and concentrated to give 75 mg of a crude material as an amber oil. The product was purified by reverse-phase HPLC and submitted direct to screening as a 30 mM solution, with 859 μL being obtained. The concentration was determined by evaporative light scattering detector (ELSD). LC-MS (APCI) *m/z* 380 (M + H)⁺; ¹H NMR (400 MHz, DMSO-*d*₆) δ 8.14 (s, 2H), 7.67–7.61 (m, 2H), 7.52–7.51 (m, 1H), 7.36–7.33 (m, 1H), 7.09–7.05 (m, 1H), 6.89–6.85 (m, 1H), 6.57 (s, 1H), 6.31 (br s, 2H), 5.52–5.50 (m, 1H), 3.34 (s, 3H), 1.59–1.58 (m, 3H).

2-(4-Methylthiazol-2-yl)propan-2-ol (19a**).** This reaction was carried out in two batches of 33.9 g, which were subsequently combined for purification. Compound **18** (33.9 g, 341.7 mmol) was dissolved in dry Et₂O (700 mL) under nitrogen and cooled to -78 °C. A solution of *n*-BuLi in heptane (2.1 M, 179.0 mL, 375.9 mmol) was added slowly from a pressure-equalizing dropping funnel over 2 h, with the internal temperature being maintained between -60 and -65 °C during the addition. After the mixture was stirred for a further 45 min at -60 °C, acetone (27.6 mL, 375.9 mmol) was added over 45 min while the reaction was maintained at this temperature. The reaction was then stirred for 30 min at -60 °C before being quenched by the careful addition of 25% ammonium acetate solution (200 mL). The mixture was extracted several times with EtOAc (1 L total), and the combined organic extracts were washed with H₂O (150 mL) and brine (150 mL), dried over MgSO₄, and concentrated to give a yellow solid. The combined batches of solid were recrystallized from hot heptane, and the solid was collected and dried to give **19a** (70 g, 65% yield) as an off-white solid. LC-MS (APCI) *m/z* 158.1 (M + H)⁺; ¹H NMR (400 MHz, CDCl₃) δ 6.78 (s, 1H), 3.15 (s, 1H), 2.41 (s, 3H), 1.64 (s, 6H).

2-(5-Bromo-4-methylthiazol-2-yl)propan-2-ol (20**).** To a solution of **19a** (70 g, 445.19 mmol) in dichloromethane (DCM; 750 mL) at 5 °C was added N-bromosuccinimide (NBS; 87.16 g, 489.71 mmol) portionwise over 20 min. After being stirred at room temperature for 2.5 h, the reaction was diluted with DCM (250 mL) and washed with 10% sodium thiosulfate solution (200 mL), H₂O (100 mL), and brine (150 mL). The organic extracts were dried over Na₂SO₄ and concentrated to give crude **20** (110 g, >100% yield) as a yellow oil, which was used without further purification. LC-MS (APCI) *m/z* 236.2 (M + H)⁺; ¹H NMR (400 MHz, CDCl₃) δ 2.37 (s, 3H), 1.63 (s, 6H), one OH proton is missing due to deuterium exchange.

Compounds **21**–**23** were synthesized via the same two-step sequence used to prepare **20**.

3-(5-Bromo-4-methylthiazol-2-yl)-1-methylazetidin-3-ol (21**).** LC-MS (APCI) *m/z* 262.95 (M + H)⁺; ¹H NMR (400 MHz, CDCl₃) δ 4.51 (br s, 1H), 3.69 (d, *J* = 9.3 Hz, 2H), 3.54 (d, *J* = 9.3 Hz, 2H), 2.44 (s, 3H), 2.32 (s, 3H).

3-(5-Bromo-4-methylthiazol-2-yl)tetrahydrofuran-3-ol (22**).** LC-MS (APCI) *m/z* 264.05 (M + H)⁺; ¹H NMR (400 MHz, CDCl₃) δ 4.14–4.05 (m, 2H), 3.94–3.85 (m, 2H), 3.28 (s, 1H), 2.52 (dt, *J* = 13.3, 8.8 Hz, 1H), 2.30 (s, 3H), 2.24–2.21 (m, 1H).

3-(5-Bromo-4-methylthiazol-2-yl)-3-hydroxytetrahydrothiophene 1,1-Dioxide (23). LC-MS (APCI) *m/z* 311.90 ($M + H$)⁺; ¹H NMR (400 MHz, CDCl₃) δ 3.70 (s, 1H), 3.65 (d, *J* = 6.6 Hz, 2H), 3.48–3.42 (m, 1H), 3.37–3.31 (m, 1H), 2.74 (ddd, *J* = 14, 11.2, 8.7 Hz, 1H), 2.53–2.47 (m, 1H), 2.30 (s, 3H).

Synthesis of 5-Bromo-2-isopropenyl-4-methylthiazole (24).

This reaction was carried out in two batches of 55 g, which were subsequently combined for workup and purification. Compound 20 (55 g, 232.92 mmol) was dissolved in acetic acid (500 mL), and concentrated H₂SO₄ (13.36 mL, 249.2 mmol) was added. The reaction mixture was then heated at 80–85 °C for 20 h. The reaction mixtures was cooled and combined, and the acetic acid was removed by distillation under reduced pressure (bp ~45 °C, ~70 mmHg). The residue was carefully neutralized by the addition of solid NaHCO₃, diluted with H₂O (400 mL), and extracted with EtOAc (3 × 750 mL). The combined organic extracts were washed with H₂O (100 mL) and brine (250 mL), dried over Na₂SO₄, and concentrated to give a brown oil. The crude oil was purified by flash chromatography over silica gel (heptane to 10% EtOAc in heptane) to give 24 (36.5 g, 36% yield) as a yellow oil. LC-MS (APCI) *m/z* 218.2 ($M + H$)⁺; ¹H NMR (400 MHz, CDCl₃) δ 5.73–5.71 (m, 1H), 5.29–5.26 (m, 1H), 2.39 (s, 3H), 2.18–2.16 (m, 3H).

Synthesis of (R)-2-(5-Bromo-4-methylthiazol-2-yl)propane-1,2-diol (26).

This reaction was carried out in two batches of 21.5 g, which were subsequently combined for workup and purification. To a solution of 24 (21.5 g, 98.5 mmol) in a mixed solvent of THF (300 mL), *t*-BuOH (300 mL), and H₂O (300 mL) was added AD-mix- α (97.5 g) in a portionwise manner with the internal temperature being maintained between 20 and 25 °C. The reaction mixture was then stirred at room temperature for 60 h. The two batches were combined, H₂O (500 mL) was added, and the mixture was extracted with EtOAc (3 × 1 L). The combined organic extracts were washed with H₂O (200 mL) and brine (500 mL), dried over Na₂SO₄, and concentrated to give a brown oil. The crude material was purified by column chromatography over silica (1/1 heptane/EtOAc) to give the enantioenriched diol as a colorless solid (41.6 g, 83% yield, 91.3% ee). Recrystallization from a mixture of EtOAc (48 mL) and heptane (240 mL) gave enantiopure 26 (26.2 g, 73% yield, 99.5% ee) as a white solid. LC-MS (APCI) *m/z* 251.9 ($M + H$)⁺; ¹H NMR (400 MHz, CDCl₃) δ 4.03 (d, *J* = 11.12 Hz, 1H), 3.68 (d, *J* = 11.12 Hz, 1H), 3.43 (s, 1H), 2.49 (s, 1H), 2.36 (s, 3H), 1.54 (s, 3H). Compound 26 was obtained in >99% ee by chiral HPLC on a Chiralpak IA 4.6 × 250 mm column, eluted with 80% heptane/20% ethanol with 0.2% diethylamine (DEA) at a flow rate of 0.7 mL/min. Retention time of 26 under these conditions is 6.63 min. The opposite enantiomer 25 has a retention time of 7.83 min. Compound 25 was synthesized in a similar manner to 26 by reacting 24 with AD-mix- β .

3-[5-(6-Amino-5-[(1*R*)-1-[5-fluoro-2-(2*H*-1,2,3-triazol-2-yl)-phenyl]ethoxy]pyridin-3-yl)-4-methyl-1,3-thiazol-2-yl]-1-methylazetidin-3-ol (8a). In a similar manner to 7h, 17 (150 mg, 0.35 mmol) was reacted with 3-(5-bromo-4-methylthiazol-2-yl)-1-methylazetidin-3-ol 21 (139 mg, 0.53 mmol) to afford 8a (17 mg, 10% yield) as a tan solid after reverse-phase HPLC. LC-MS (APCI) *m/z* 482.1 ($M + H$)⁺; ¹H NMR (400 MHz, DMSO-*d*₆) δ 8.19 (s, 2H), 7.67 (dd, *J* = 8.97, 5.18 Hz, 1H), 7.61 (dd, *J* = 9.73, 2.91 Hz, 1H), 7.53 (d, *J* = 1.77 Hz, 1H), 7.39–7.30 (m, 1H), 6.67 (br s, 1H), 6.63 (d, *J* = 2.02 Hz, 1H), 6.21 (br s, 2H), 5.59 (q, *J* = 6.12 Hz, 1H), 3.62 (d, *J* = 8.08 Hz, 2H), 3.30 (d, *J* = 8.08 Hz, 2H), 2.32 (s, 3H), 2.11 (s, 3H), 1.57 (d, *J* = 6.12 Hz, 3H).

3-[5-(6-Amino-5-[(1*R*)-1-[5-fluoro-2-(2*H*-1,2,3-triazol-2-yl)-phenyl]ethoxy]pyridin-3-yl)-4-methyl-1,3-thiazol-2-yl]-tetrahydrofuran-3-ol (8b). In a similar manner to 7h, 17 (115 mg, 0.27 mmol) was reacted with 3-(5-bromo-4-methylthiazol-2-yl)-tetrahydrofuran-3-ol 22 (107 mg, 0.41 mmol) to afford a racemic product (51 mg, 39% yield) as a tan solid after reverse-phase HPLC. Chiral separation was carried out by SFC on an AD-H column (4.6 × 250 mm), eluted with 30% MeOH @140 bar with a flow rate of 3 mL/min. Compound 8b was obtained as peak 2 (6.67 min) and the inactive enantiomer as peak 1 (4.10 min). LC-MS (APCI) *m/z* 483.1 ($M + H$)⁺; ¹H NMR (400 MHz, DMSO-*d*₆) δ 8.20 (s, 2H), 7.68 (dd, *J* = 9.0, 5.2 Hz, 1H), 7.61 (dd, *J* = 9.7, 2.9 Hz, 1H), 7.53 (d, *J* = 1.8 Hz, 1H), 7.36 (td, *J* = 8.4, 2.9 Hz, 1H), 6.63 (d, *J* = 1.5 Hz, 1H), 6.33 (s, 1H), 6.20 (br s, 2H),

5.61 (q, *J* = 5.6 Hz, 1H), 4.05–3.94 (m, 2H), 3.93–3.76 (m, 2H), 2.49–2.35 (m, 1H), 2.20–2.10 (m, 1H), 2.07 (s, 3H), 1.58 (d, *J* = 6.3 Hz, 3H).

3-[5-(6-Amino-5-[(1*R*)-1-[5-fluoro-2-(2*H*-1,2,3-triazol-2-yl)-phenyl]ethoxy]pyridin-3-yl)-4-methyl-1,3-thiazol-2-yl]-tetrahydrothiophene-3-ol 1,1-Dioxide (8c). Compound 17 (1.38 g, 3.24 mmol), 3-(5-bromo-4-methylthiazol-2-yl)-3-hydroxytetrahydrothiophene 1,1-dioxide 23 (1.35 g, 4.33 mmol), and cesium fluoride (1.55 g, 10.1 mmol) were combined, and methanol (4 mL) was added. The solution was thoroughly degassed before bis[di-*tert*-butyl(4-dimethylaminophenyl)phosphine]dichloropalladium(II) (Pd-132, 102 mg, 0.14 mmol) was added. After being heated at 50 °C for 1 h, the reaction was concentrated, taken up in EtOAc, washed with water, dried over Na₂SO₄, and concentrated. The residue was purified by column chromatography over silica gel (0–100% EtOAc in heptane) to afford a racemic product (1.15 g, 65%) as a yellow foam. Chiral separation was carried out by SFC on an AD-H column (4.6 × 250 mm) eluting with 50% MeOH @120 bar with a flow rate of 5 mL/min. Compound 8c was obtained as peak 1 (0.53 min) and the inactive enantiomer as peak 2 (1.67 min). LC-MS (APCI) *m/z* 531.1 ($M + H$)⁺; ¹H NMR (400 MHz, DMSO-*d*₆) δ 8.20 (s, 2H), 7.70–7.59 (m, 2H), 7.55 (d, *J* = 1.77 Hz, 1H), 7.40–7.31 (m, 1H), 7.03 (s, 1H), 6.64 (d, *J* = 1.77 Hz, 1H), 6.25 (br s, 2H), 5.64–5.56 (m, 1H), 3.61–3.54 (m, 1H), 3.51–3.33 (m, 3H), 2.59–2.40 (m, 2H), 2.11 (s, 3H), 1.58 (d, *J* = 6.32 Hz, 3H).

5-(6-Amino-5-[(1*R*)-1-[5-fluoro-2-(2*H*-1,2,3-triazol-2-yl)-phenyl]ethoxy]pyridin-3-yl)-2-[(2*R*)-1,2-dihydroxypropan-2-yl]-1,3-thiazole-4-carbonitrile (8e). In a sealed vessel, 17 (11.6 g, 27.3 mmol) was combined with 26 (6.88 g, 27.3 mmol), Pd(dppf)Cl₂ (1.05 g, 1.36 mol), cesium fluoride (14.5 g, 95.5 mmol), and methanol (300 mL). After the reaction mixture was heated at 120 °C for 1 h, it was concentrated and partitioned between EtOAc and water. The dark insoluble materials were filtered off. The organic layer was dried over Na₂SO₄, filtered, and concentrated to give a dark brown oil. The oil was preabsorbed onto silica and purified by column chromatography, eluted with 0–10% MeOH in DCM, to give 8e as a brown foam. This foam was stirred in water for 1 h and then filtered under vacuum and washed with more water. After being dried under vacuum at 60 °C for 18 h, 8e was obtained as a free-flowing tan powder (7.78 g, 61% yield). LC-MS (APCI) *m/z* 471.1 ($M + H$)⁺; ¹H NMR (400 MHz, DMSO-*d*₆) δ 8.20 (s, 2H), 7.67 (dd, *J* = 8.72, 5.18 Hz, 1H), 7.61 (dd, *J* = 9.60, 2.78 Hz, 1H), 7.52 (d, *J* = 1.52 Hz, 1H), 7.34 (td, *J* = 8.4, 2.9 Hz, 1H), 6.62 (d, *J* = 1.26 Hz, 1H), 6.17 (br s, 2H), 5.70 (s, 1H), 5.61 (q, *J* = 6.30 Hz, 1H), 4.83 (t, *J* = 6.06 Hz, 1H), 3.51 (d, *J* = 6.06 Hz, 2H), 2.07 (s, 3H), 1.58 (d, *J* = 6.06 Hz, 3H), 1.41 (s, 3H); ¹³C NMR (101 MHz, DMSO-*d*₆) δ 174.52, 162.28 (*J*_{F-C} = 246 Hz), 150.65, 145.63, 139.78 (*J*_{F-C} = 7.0 Hz), 138.67, 138.14, 136.51, 133.80 (*J*_{F-C} = 3.0 Hz), 128.37, 127.88 (*J*_{F-C} = 9.0 Hz), 117.05, 115.96, 115.93 (*J*_{F-C} = 23 Hz), 113.23 (*J*_{F-C} = 24 Hz), 75.01, 70.02, 69.39, 25.10, 23.01, 15.66; ¹⁹F NMR (377 MHz, DMSO-*d*₆) δ –110.68 (note that it is negative relative to the reference CFCl₃ at 0 ppm for ¹⁹F).

5-(6-Amino-5-[(1*R*)-1-[5-fluoro-2-(2*H*-1,2,3-triazol-2-yl)-phenyl]ethoxy]pyridin-3-yl)-2-[(2*S*)-1,2-dihydroxypropan-2-yl]-1,3-thiazole-4-carbonitrile (8d). Compound 8d was prepared in a similar manner to 8e, with 25 as opposed to 26 in the Suzuki coupling reaction. LC-MS (APCI) *m/z* 471.1 ($M + H$)⁺; ¹H NMR (400 MHz, DMSO-*d*₆) δ 8.20 (s, 2H), 7.69 (dd, *J* = 8.8, 5.1 Hz, 1H), 7.63 (dd, *J* = 9.7, 2.9 Hz, 1H), 7.53 (d, *J* = 2 Hz, 1H), 7.36 (td, *J* = 8.4, 2.9 Hz, 1H), 6.63 (d, *J* = 1.9 Hz, 1H), 6.17 (br s, 2H), 5.71 (s, 1H), 5.62 (q, *J* = 6.3 Hz, 1H), 4.84 (t, *J* = 6.2 Hz, 1H), 3.52 (d, *J* = 6.1 Hz, 2H), 2.09 (s, 3H), 1.58 (d, *J* = 6.3 Hz, 3H), 1.42 (s, 3H).

Co-crystal Structures. The co-crystal structures described for the first time here have been deposited to the Protein Data Bank (wwPDB), and the details of the methods used can be found under accession codes 4ccb (wt ALK + 6d, 2.0 Å), 4ccu (wt ALK + 7h, 2.0 Å), and 4cd0 (L1196M ALK + 8e, 2.2 Å). Nonphosphorylated human wt and L1196M mutant ALK kinase domain proteins (amino acids 1093–1411) were crystallized by the hanging drop vapor diffusion method at 13 °C by mixing equal volumes of a purified protein (11–15 mg/mL)–inhibitor (~1.0 mM) complex solution with a crystallization solution containing 0.15 M ammonium sulfate, 9–10.5% (w/v) monomethyl ether poly(ethylene glycol) (MW 5000), and 0.1 M 2-(*N*-morpholino)-

ethanesulfonic acid (MES) buffer in a pH range of 5.3–5.6 for wt ALK or 0.2 M lithium sulfate, 18% (w/v) poly(ethylene glycol) (MW 5000), and 0.1 M Tris at pH 8.5 for L1196M ALK.

Biochemical Kinase Assays. Recombinant human wild-type and L1196M mutant ALK kinase domain proteins (amino acids 1093–1411) were produced in-house in a baculoviral expression system and preactivated via autophosphorylation. Enzymes were assayed for kinase activity by a microfluidic mobility shift assay. The reactions were conducted in 50- μ L volumes in 96-well plates and contained 1.3 nM wild-type or 0.5 nM mutant ALK, 3 μ M phosphoacceptor peptide (5'FAM-KKSRGDYMTMQIG-CONH₂, synthesized by CPC Scientific, Sunnyvale, CA), test compound (11-dose 3-fold serial dilutions, 2% DMSO final) or DMSO only, 1 mM dithiothreitol (DTT), 0.002% Tween-20, and 5 mM MgCl₂ in 25 mM N-(2-hydroxyethyl)piperazine-N'-ethanesulfonic acid (Hepes), pH 7.1, and were initiated by addition of ATP at the $K_{M,app}$ level (53 and 51 μ M for wild-type and L1196M ALK, respectively), following a 15-min preincubation. The reactions were incubated for 1 h at room temperature, stopped by the addition of equal volume of ethylenediaminetetraacetic acid (EDTA), pH 8 (0.1 M final concentration), and the extent of reactions (~15–20% conversion with no inhibitor) was determined after electrophoretic separation of the fluorescently labeled peptide substrate and phosphorylated product on a LabChip EZ Reader II (Caliper Life Sciences, Hopkinton, MA). The inhibitors were shown to be ATP-competitive from kinetic and crystallographic studies. The K_i values were calculated by fitting the percent conversion to the Morrison equation for tight-binding competitive inhibition by a nonlinear regression method (GraphPad Prism, GraphPad Software, San Diego, CA).

Kinase Selectivity Enzyme Assays. The experiments were conducted by Invitrogen Inc. (Carlsbad, CA) in their Madison, WI facility. Most of the kinase panel assays were the fluorescence resonance energy transfer (FRET)-based Z-LYTE assays that employ a fluorescence-based, coupled-enzyme format, taking advantage of the differential sensitivity of phosphorylated and nonphosphorylated peptides to proteolytic cleavage. Other assays were the time-resolved (TR) FRET-based Adapta assay format that employs an Alexa Fluor 647-labeled ADP tracer and Eu-labeled anti-ADP antibody. The assays of the above two formats were normally conducted with ATP concentration near $K_{M,app}$. Another assay format used was the TR-FRET-based LanthaScreen binding assays utilizing an Alexa Fluor tracer and Eu-labeled anti-tag antibody that binds to the respective affinity tag of the target kinase. Details of these assay procedures are described on the vendor's Web site.

Cell-Based Phospho-ALK Enzyme-Linked Immunosorbent Assay. Cells were seeded at 20 000 cells/well in a 96-well plate in growth medium with 0.5% serum and incubated overnight. Compounds were diluted in medium without serum, added to the cells, incubated for 1 h, and then removed by aspirating the medium by vacuum suction. Cell lysates were generated and the phospho-ALK (Tyr1604) levels were determined by use of the PathScan Phospho-ALK (Tyr1604) Chemiluminescent Sandwich ELISA Kit (Cell Signaling, catalog no. 7020) or PathScan Total ALK Chemiluminescent Sandwich ELISA Kit (Cell Signaling, catalog no. 7084) as described in the manufacturer's protocol. IC₅₀ values were calculated by concentration–response curve fitting utilizing a four-parameter analytical method.

Tumor Cell Proliferation Assay. Cells were seeded in 96-well plates in growth medium + 10% fetal bovine serum (FBS) (50 mL) and cultured overnight at 37 °C. The following day, serial dilutions of 8e or appropriate controls were added to the designated wells, and cells were incubated at 37 °C for 72 h. A Cell Titer Glo assay (Promega, Madison, WI) was then performed to determine the relative cell numbers. IC₅₀ values were calculated by concentration–response curve fitting utilizing a four-parameter analytical method.

In Vivo Xenograft Models in Athymic Mice. Female nu/nu mice were obtained from Charles River. All of the procedures were conducted in accordance with the Institute for Laboratory Animal Research Guide for the Care and Use of Laboratory Animals and with Pfizer Animal Care and Use Committee guidelines. Tumor cells were implanted subcutaneously into the right flank region of each mouse and allowed to grow to the designated size. The athymic mice bearing established

tumors were administered 8e by oral gavage in 0.5% methylcellulose suspension or 0.5% methylcellulose solution alone for the control group. Tumor volume was measured by use of electronic digital calipers.

ASSOCIATED CONTENT

Supporting Information

One table listing additional experimental details of biochemical kinase selectivity for 8e, and SMILES molecular formula strings and compound data information in a csv file. This material is available free of charge via the Internet at <http://pubs.acs.org>.

Accession Codes

ALK kinase domain crystal structures deposited to the Protein Data Bank (wwPDB) are wt–crizotinib (2xp2), L1196M (2yhv), L1196M–crizotinib (2yfx), G1269A (4anl), G1269A–crizotinib (4anq), wt–6d (4ccb), wt–7h (4ccu), and L1196M–8e (4cd0).

AUTHOR INFORMATION

Corresponding Authors

*Phone (858)-622-3165; e-mail qinhua.huang@pfizer.com.
*Phone (858)-526-4683; e-mail ted.w.johnson@pfizer.com.

Notes

The authors declare no competing financial interest.

ACKNOWLEDGMENTS

We are grateful to Dr. Klaus Dress for helpful data analyses and discussions.

ABBREVIATIONS USED

ADME, absorption, distribution, metabolism, and excretion; ALCL, anaplastic large-cell lymphoma; ALK, anaplastic lymphoma kinase; c-MET, mesenchymal epithelial transition factor; DLBCL, diffuse large B-cell lymphoma; EML4, echinoderm microtubule associated protein-like 4; G-loop, glycine loop; HLM, human liver microsome; HPLC, high-performance liquid chromatography; IC₅₀, 50% inhibitory concentration; LipE, lipophilicity efficiency; log D, octanol/buffer (pH 7.4) distribution coefficient; IMT, myofibroblastic tumor; IR, insulin receptor; NPM, nucleophosmin; NSCLC, non-small-cell lung cancer; PK, pharmacokinetic; RTK, receptor tyrosine kinase; SBDD, structure-based drug design; SFC, supercritical fluid chromatography; wt, wild type

REFERENCES

- (1) Morris, S. W.; Naeve, C.; Mathew, P.; James, P. L.; Kirstein, M. N.; Cui, X.; Witte, D. P. ALK, the chromosome 2 gene locus altered by the t(2;5) in non-Hodgkin's lymphoma, encodes a novel neural receptor tyrosine kinase that is highly related to leukocyte tyrosine kinase (LTK). *Oncogene* 1997, 14, 2175–2188.
- (2) Bilsland, J. G.; Wheeldon, A.; Mead, A.; Znamenskiy, P.; Almond, S.; Waters, K. A.; Thakur, M.; Beaumont, V.; Bonnert, T. P.; Heavens, R.; Whiting, P.; McAllister, G.; Munoz-Sanjuan, I. Behavioral and neurochemical alterations in mice deficient in anaplastic lymphoma kinase suggest therapeutic potential for psychiatric indications. *Neuropsychopharmacology* 2008, 33, 685–700.
- (3) (a) Chiarle, R.; Voena, C.; Ambrogio, C.; Piva, R.; Inghirami, G. The anaplastic lymphoma kinase in the pathogenesis of cancer. *Nat. Rev. Cancer* 2008, 8, 11–23. (b) Webb, T. R.; Slavish, J.; George, R. E.; Look, A. T.; Xue, L.; Jiang, Q.; Cui, X.; Rentrop, W. B.; Morris, S. W. Anaplastic lymphoma kinase: role in cancer pathogenesis and small-molecule inhibitor development for therapy. *Expert Rev. Anticancer Ther.* 2009, 9, 331–356. (c) Iwahara, T.; Fujimoto, J.; Wen, D.; Cupples, R.; Bucay, N.; Arakawa, T.; Mori, S.; Ratzkin, B.; Yamamoto, T. Molecular characterization of ALK, a receptor tyrosine kinase expressed specifically in the nervous system. *Oncogene* 1997, 14, 439–449.

- (4) Morris, S. W.; Kirstein, M. N.; Valentine, M. B.; Dittmer, K. G.; Shapiro, D. N.; Saltman, D. L.; Look, A. T. Fusion of a kinase gene, ALK, to a nucleolar protein gene, NPM, in non-Hodgkin's lymphoma. *Science* **1994**, *263*, 1281–1284.
- (5) Yu, H.; Liu, X.; Li, H.; Shi, D.; Wang, C. ALK-positive large B-cell lymphoma: report of two cases and review of the literature. *J. Cancer Sci. Ther.* **2011**, *3*, 228–232.
- (6) Griffin, C. A.; Hawkins, A. L.; Dvorak, C.; Henkle, C.; Ellingham, T.; Perlman, E. J. Recurrent involvement of 2p23 in inflammatory myofibroblastic tumors. *Cancer Res.* **1999**, *59*, 2776–2780.
- (7) (a) Soda, M.; Choi, Y. L.; Enomoto, M.; Takada, S.; Yamashita, Y.; Ishikawa, S.; Fujiwara, S.; Watanabe, H.; Kurashina, K.; Hatanaka, H.; Bando, M.; Ohno, S.; Ishikawa, Y.; Aburatani, H.; Niki, T.; Sohara, Y.; Sugiyama, Y.; Mano, H. Identification of the transforming EML4–ALK fusion gene in non-small-cell lung cancer. *Nature* **2007**, *448*, 561–566. (b) Mano, H. Non-solid oncogenes in solid tumors: EML4–ALK fusion genes in lung cancer. *Cancer Sci.* **2008**, *99*, 2349–2355. (c) Shaw, A. T.; Solomon, B. Targeting anaplastic lymphoma kinase in lung cancer. *Clin. Cancer Res.* **2011**, *17*, 2081–2086.
- (8) (a) Caren, H.; Abel, F.; Kogner, P.; Martinsson, I. High incidence of DNA mutations and gene amplifications of the ALK gene in advanced sporadic neuroblastoma tumors. *Biochem. J.* **2008**, *416*, 153–159. (b) Mossé, Y. P.; Laudenslager, M.; Longo, L.; Cole, K. A.; Wood, A.; Attiyeh, E. F.; Laquaglia, M. J.; Sennett, R.; Lynch, J. E.; Perri, P.; Laureys, G.; Speleman, F.; Kim, C.; Hou, C.; Hakonarson, H.; Torkamani, A.; Schork, N. J.; Brodeur, G. M.; Tonini, G. P.; Rappaport, E.; Devoto, M.; Maris, J. M. Identification of ALK as a major familial neuroblastoma predisposition gene. *Nature* **2008**, *455*, 930–935. (c) Janoueix-Lerosey, I.; Lequin, D.; Brugieres, L.; Ribeiro, A.; de Pontual, L.; Combaret, V.; Raynal, V.; Puiseux, A.; Schleiermacher, G.; Pierron, G.; Valteau-Couanet, D.; Frebourg, T.; Michon, J.; Lyonnet, S.; Amiel, J.; Delattre, O. Somatic and germline activating mutations of the ALK kinase receptor in neuroblastoma. *Nature* **2008**, *455*, 967–970. (d) Chen, Y.; Takita, J.; Choi, Y. L.; Kato, M.; Ohira, M.; Sanada, M.; Wang, Li.; Soda, M.; Kikuchi, A.; Igarashi, T.; Nakagawara, A.; Hayashi, Y.; Mano, H.; Ogawa, S. Oncogenic mutations of ALK kinase in neuroblastoma. *Nature* **2008**, *455*, 971–974. (e) George, R. E.; Sanda, T.; Hanna, M.; Frohling, S.; Luther, W., 2nd; Zhang, J.; Ahn, Y.; Zhou, W.; London, W. B.; McGrady, P.; Xue, L.; Zozulya, S.; Gregor, V.; Webb, T. R.; Nathanael, S.; Gray, N. S.; Gilliland, D. G.; Diller, L.; Greulich, H.; Stephan, W.; Morris, S. W.; Meyerson, M.; Look, A. T. Activating mutations in ALK provides a therapeutic target in neuroblastoma. *Nature* **2008**, *455*, 975–978. (f) Azarova, A. M.; Gautam, G.; George, R. E. Emerging importance of ALK in neuroblastoma. *Semin. Cancer Biol.* **2011**, *21*, 267–275.
- (9) Tuma, R. S. ALK gene amplified in most inflammatory breast cancers. *J. Natl. Cancer Inst.* **2012**, *104*, 87–88.
- (10) Ren, H.; Tan, X. Z.; Crosby, C.; Haack, H.; Ren, J.-M.; Beausoleil, S.; Moritz, A.; Innocenti, G.; Rush, J.; Zhang, Y.; Zhou, X.-M.; Gu, T.-L.; Yang, Y.-F.; Comb, M. J. Identification of anaplastic lymphoma kinase as a potential therapeutic target in ovarian cancer. *Cancer Res.* **2012**, *72*, 3312–3323.
- (11) (a) Zou, H. Y.; Li, Q.; Lee, J. H.; Arango, M. E.; McDonnell, S. R.; Yamazaki, S.; Koudriakova, T. B.; Alton, G.; Cui, J. J.; Kung, P.-P.; Nambu, M. D.; Los, G.; Bender, B. L.; Mroczkowski, B.; Christensen, J. G. An orally available small-molecule inhibitor of c-MET, PF-2341066, exhibits cytoreductive antitumor efficacy through antiproliferative and antiangiogenic mechanisms. *Cancer Res.* **2007**, *67*, 4408–4417. (b) Christensen, J. G.; Zou, H. Y.; Arango, M. E.; Li, Q.; Lee, J. H.; McDonnell, S. R.; Yamazaki, S.; Alton, G.; Mroczkowski, B.; Christensen, J. G. Cytoreductive antitumor activity of PF-2341066, a novel inhibitor of anaplastic lymphoma kinase and c-MET, in experimental models of anaplastic large-cell lymphoma. *Mol. Cancer Ther.* **2007**, *6*, 3314–3322. (c) Cui, J. J.; Tran-Dube, M.; Shen, H.; Nambu, M.; Kung, P.-P.; Pairish, M.; Jia, L.; Meng, J.; Funk, L.; Botrous, I.; McTigue, M.; Grodsky, N.; Ryan, K.; Padrique, E.; Alton, G.; Timofeevskii, S.; Yamazaki, S.; Li, Q.; Zou, H.; Christensen, J.; Mroczkowski, B.; Bender, S.; Kania, R. S.; Edwards, M. P. Structure based drug design of crizotinib (PF-02341066), a potent and selective dual inhibitor of mesenchymal–epithelial transition factor (c-MET) kinase and anaplastic lymphoma kinase (ALK). *J. Med. Chem.* **2011**, *54*, 6342–6363. (d) Cui, J. J.; McTigue, M.; Kania, R. S.; Edwards, M. P. Case History: XalkoriTM (crizotinib), a potent and selective dual inhibitor of mesenchymal epithelial transition (MET) and anaplastic lymphoma kinase (ALK) for cancer treatment. *Annu. Rep. Med. Chem.* **2013**, *48*, 421–432.
- (12) Shaw, A. T.; Yeap, B. Y.; Solomon, B. J.; Riely, G. J.; Gainor, J.; Engelman, J. A.; Shapiro, G. I.; Costa, D. B.; Ou, S.-H. I.; Butaney, M.; Salgia, R.; Maki, R. G.; Varella-Garcia, M.; Doebele, R. C.; Bang, Y.-J.; Kulig, K.; Selaru, P.; Tang, Y.; Wilner, K. D.; Kwak, E. L.; Clark, J. W.; Iafrate, A. J.; Camidge, D. R. Effect of crizotinib on overall survival in patients with advanced non-small-cell lung cancer harbouring ALK gene rearrangement: a retrospective analysis. *Lancet Oncol.* **2011**, *12*, 1004–1012.
- (13) (a) Choi, Y. L.; Soda, M.; Yamashita, Y.; Ueno, T.; Takashima, J.; Nakajima, T.; Yatabe, Y.; Takeuchi, K.; Hamada, T.; Haruta, H.; Ishikawa, Y.; Kimura, H.; Mitsudomi, T.; Tanio, Y.; Mano, H. EML4–ALK mutations in lung cancer that confer resistance to ALK inhibitors. *N. Engl. J. Med.* **2010**, *363*, 1734–1739. (b) Sasaki, T.; Okuda, K.; Zheng, W.; Butrynski, J.; Capelletti, M.; Wang, L.; Gray, N. S.; Wilner, K.; Christensen, J. G.; Demetri, G.; Shapiro, G. I.; Rodig, S. J.; Eck, M. J.; Jänne, P. A. A novel ALK secondary mutation and EGFR signaling cause resistance to ALK kinase inhibitors. *Cancer Res.* **2011**, *71*, 6051–6060. (c) Zhang, S.; Wang, F.; Keats, J.; Zhu, X.; Ning, Y.; Wardwell, S. D.; Moran, L.; Mohammad, Q. K.; Anjum, R.; Wang, Y.; Narasimhan, N. I.; Dalgarino, D.; Shakespeare, W. C.; Miret, J. J.; Clackson, T.; Rivera, V. M. Crizotinib-resistant mutants of EML4–ALK identified through an accelerated mutagenesis screen. *Chem. Biol. Drug Des.* **2011**, *78*, 999–1005. (d) Doebele, R. C.; Pilling, A. B.; Aisner, D. L.; Kutateladze, T. G.; Le, A. T.; Weickhardt, A. J.; Kondo, K. L.; Linderman, D. J.; Heasley, L. E.; Franklin, W. A.; Varella-Garcia, M.; Camidge, D. R. Mechanisms of resistance to crizotinib in patients with ALK gene rearranged non-small cell lung cancer. *Clin. Cancer Res.* **2012**, *18*, 1472–1482. (e) Katayama, R.; Shaw, A. T.; Khan, T. M.; Mino-Kenudson, M.; Solomon, B. J.; Halmos, B.; Jessop, N. A.; Wain, J. C.; Yeo, A. T.; Benes, C.; Drew, L.; Saeh, J. C.; Crosby, K.; Sequist, L. V.; Iafrate, A. J.; Engelman, J. A. Mechanisms of acquired crizotinib resistance in ALK-rearranged lung cancer. *Sci. Transl. Med.* **2012**, *4*, No. 120ra17. (f) Kinoshita, K.; Oikawa, N.; Tsukuda, T. Anaplastic lymphoma kinase inhibitors for the treatment of ALK-positive cancers. *Annu. Rep. Med. Chem.* **2012**, *47*, 281–293.
- (14) (a) Galkin, A. V.; Melnick, J. S.; Kim, S.; Hood, T. L.; Li, N.; Li, L.; Xia, G.; Steensma, R.; Chopiu, G.; Jiang, J.; Wan, Y.; Ding, P.; Liu, Y.; Sun, F.; Schultz, P. G.; Gray, N. S.; Warmuth, M. Identification of NVP-TAE684, a potent, selective, and efficacious inhibitor of NPM-ALK. *Proc. Natl. Acad. Sci. U.S.A.* **2007**, *104*, 270–275. (b) Marsilje, T. H.; Pei, W.; Chen, B.; Lu, W.; Uno, T.; Jin, Y.; Jiang, T.; Kim, S.; Li, N.; Warmuth, M.; Sarkisova, Y.; Sun, F.; Steffy, A.; Pferdekamper, A. C.; Li, A. G.; Joseph, S. B.; Kim, Y.; Liu, B.; Tuntland, T.; Cui, X.; Gray, N. S.; Steensma, R.; Wan, Y.; Jiang, J.; Chopiu, G.; Li, J.; Gordon, W. P.; Richmond, W.; Johnson, K.; Chang, J.; Groessl, T.; He, Y.-Q.; Phimister, A.; Aycinena, A.; Lee, C. C.; Bursulaya, B.; Karanewsky, D. S.; Seidel, H. M.; Harris, J. L.; Michellys, P.-Y. Synthesis, structure–activity relationships, and in vivo efficacy of the novel potent and selective anaplastic lymphoma kinase (ALK) inhibitor 5-chloro-N2-(2-isopropoxy-5-methyl-4-(piperidin-4-yl)phenyl)-N4-(2-(isopropylsulfonyl)-phenyl)pyrimidine-2,4-diamine (LDK378) currently in phase 1 and phase 2 clinical trials. *J. Med. Chem.* **2013**, *56*, 5675–5690.
- (15) Kuromitsu, S.; Mori, M.; Shimada, I.; Kondoh, Y.; Shindoh, N.; Soga, T.; Furutani, T.; Konagai, S.; Sakagami, H.; Nakata, M.; Ueno, Y.; Saito, R.; Sasamata, M.; Kudou, M. Anti-tumor activity of ASP3026, a novel and selective ALK inhibitor of anaplastic lymphoma kinase (ALK). Presented at the Annual Meeting of the American Association for Cancer Research (AACR), Orlando, FL, 2011; Abstract 2821.
- (16) (a) Sakamoto, H.; Tsukaguchi, T.; Hiroshima, S.; Kodama, T.; Kobayashi, T.; Fukami, T. A.; Oikawa, N.; Tsukuda, T.; Ishii, N.; Aoki, Y. CH5424802, a selective ALK inhibitor capable of blocking the resistant gatekeeper mutant. *Cancer Cell* **2011**, *19*, 679–690. (b) Kinoshita, K;

Kobayashi, T.; Asoh, K.; Furuichi, N.; Ito, T.; Kawada, H.; Hara, S.; Ohwada, J.; Hattori, K.; Miyagi, T.; Hong, W.-S.; Park, M.-J.; Takanashi, K.; Tsukaguchi, T.; Sakamoto, H.; Tsukuda, T.; Oikawa, N. 9-Substituted 6,6-dimethyl-11-oxo-6,11-dihydro-5H-benzo[b]carbazoles as highly selective and potent anaplastic lymphoma kinase inhibitors. *J. Med. Chem.* **2011**, *54*, 6286–6294.

(17) Katayama, R.; Khan, T. M.; Benes, C.; Lifshits, E.; Eb, H.; River, V. M.; Shakespeare, W. C.; Iafrate, A. J.; Jeffrey, A.; Engelman, J. A.; Shaw, A. T. Therapeutic strategies to overcome crizotinib resistance in non-small cell lung cancers harboring the fusion oncogene EML4-ALK. *Proc. Natl. Acad. Sci. U.S.A.* **2011**, *108*, 7535–7540.

(18) (a) Edwards, M. P.; Price, D. A. Role of physicochemical properties and ligand lipophilicity efficiency in addressing drug safety risks. *Annu. Rep. Med. Chem.* **2010**, *45*, 381–391. (b) Freeman-cook, K. D.; Hoffman, R. L.; Johnson, T. W. Lipophilic efficiency: the most important efficiency metric in medicinal chemistry. *Future Med. Chem.* **2013**, *5*, 113–115.

(19) Crizotinib has an extensive tumor distribution profiles with an approximate tumor/plasma AUC ratio of 4 at steady-state (in-house data). Also see Yamazaki, S. Translational pharmacokinetic-pharmacodynamic modeling from nonclinical to clinical development: a case study of anticancer drug, crizotinib. *AAPS J.* **2013**, *15*, 354–366.

(20) Lombardo, F.; Shalaeva, M. Y.; Tupper, K. A.; Gao, F. ElogD(oct): a tool for lipophilicity determination in drug discovery. 2. Basic and neutral compounds. *J. Med. Chem.* **2001**, *44*, 2490–2497.

(21) Hosea, N. A.; Collard, W. T.; Cole, S.; Maurer, T. S.; Fang, R. X.; Jones, H.; Kakar, S. M.; Nakai, Y.; Smith, B. J.; Webster, R.; Beaumont, K. Prediction of human pharmacokinetics from preclinical information: comparative accuracy of quantitative prediction approaches. *J. Clin. Pharmacol.* **2009**, *49*, 513–533.

(22) Di, L.; Whitney, C.; Umland, J. P.; Zhang, H.; Zhang, X.; Gebhard, D. F.; Lai, Y.; Federico, J. J.; Davidson, R. E.; Smith, R.; Reyner, E. L.; Lee, C.; Feng, B.; Rotter, C.; Varma, M. V.; Kempshall, S.; Fenner, K.; El-Kattan, A. F.; Liston, T. E.; Troutman, M. D. Development of a new permeability assay using low-efflux MDCKII cells. *J. Pharm. Sci.* **2011**, *100*, 4974–4985.

(23) (a) Nishio, M.; Hirota, M.; Umezawa, Y., Eds. *The CH-Pi Interaction: Evidence, Nature, and Consequences*; Wiley-VCH: New York, 1998; pp 1–215. (b) Nishio, M. CH/π hydrogen bonds in crystals. *CrystEngComm* **2004**, *6*, 130–158.

(24) (a) Gainor, J. F.; Shaw, A. T. Novel target in non-small cell lung cancer: ROS1 and RET fusions. *Oncologist* **2013**, *18*, 865–875. (b) Chin, L. P.; Soo, R. A.; Soong, R.; Ou, S. H. Targeting ROS1 with anaplastic lymphoma kinase inhibitors: a promising therapeutic strategy for a newly defined molecular subset of non-small-cell lung cancer. *J. Thorac. Oncol.* **2012**, *7*, 1625–1630.

(25) (a) Brown, H. C.; Chandrasekharan, J.; Ramachandran, P. V. Chiral synthesis via organoboranes. 14. Selective reductions. 41. Diisopinocampheylchloroborane, an exceptionally efficient chiral reducing agent. *J. Am. Chem. Soc.* **1988**, *110*, 1539–1546. (b) Ramachandran, P. V.; Gong, B.; Brown, H. C. A remarkable inversion in configuration of the product alcohols from the asymmetric reduction of *ortho*-hydroxyacetophenones with β-chlorodiisopinocampheylborane. *Tetrahedron Lett.* **1994**, *35*, 2141–2144.

(26) (a) Kolb, H. C.; Van Nieuwenhze, M. S.; Sharpless, K. B. Catalytic asymmetric dihydroxylation. *Chem. Rev.* **1994**, *94*, 2483–2547. (b) Noe, M. C.; Letavic, M. A.; Snow, S. L. Asymmetric dihydroxylation of alkenes. *Org. React.* **2005**, *66*, 109.

■ NOTE ADDED AFTER ASAP PUBLICATION

This manuscript was published ASAP on February 6, 2014, without a Supporting Information csv file. The revised version with the Supporting Information csv file was posted on February 13, 2014.